HHS Public Access

Author manuscript

Cell Rep. Author manuscript; available in PMC 2019 February 15.

Published in final edited form as:

Cell Rep. 2019 January 29; 26(5): 1174–1188.e5. doi:10.1016/j.celrep.2019.01.032.

Enhancer Histone Acetylation Modulates Transcriptional Bursting Dynamics of Neuronal Activity-Inducible Genes

Liang-Fu Chen[1], **Yen Ting Lin**[2], **David A. Gallegos**[1], **Mariah F. Hazlett**[1], **Mariana Gómez-Schiavon**[3,4,5], **Marty G. Yang**[1], **Breanna Kalmeta**[1], **Allen S. Zhou**[1], **Liad Holtzman**[4,6], **Charles A. Gersbach**[4,6,7], **Jörg Grandl**[1], **Nicolas E. Buchler**[4,5,8,*], and **Anne E. West**[1,9,*]

[1]Department of Neurobiology, Duke University, Durham, NC 27710, USA

[2]Center for Nonlinear Studies (T-CNLS) and Theoretical Biology and Biophysics Group (T-6), Theoretical Division, Los Alamos National Laboratory, NM 87545, USA

[3]Program in Computational Biology and Bioinformatics, Duke University, Durham, NC 27710, USA

[4]Center for Genomic and Computational Biology, Duke University, Durham, NC 27710, USA

[5]Department of Biology, Duke University, Durham, NC 27710, USA

[6]Department of Biomedical Engineering, Duke University, Durham, NC 27710, USA

[7]Department of Orthopaedic Surgery, Duke University, Durham, NC 27710, USA

[8]Department of Molecular Biomedical Sciences, North Carolina State University, Raleigh, NC 27606, USA

[9]Lead Contact

SUMMARY

Neuronal activity-inducible gene transcription correlates with rapid and transient increases in histone acetylation at promoters and enhancers of activity-regulated genes. Exactly how histone acetylation modulates transcription of these genes has remained unknown. We used single-cell *in situ* transcriptional analysis to show that *Fos* and *Npas4* are transcribed in stochastic bursts in mouse neurons and that membrane depolarization increases mRNA expression by increasing burst frequency. We then expressed dCas9-p300 or dCas9-HDAC8 fusion proteins to mimic or block activity-induced histone acetylation locally at enhancers. Adding histone acetylation increased *Fos*

*Correspondence: nebuchle@ncsu.edu (N.E.B.), west@neuro.duke.edu (A.E.W.).

AUTHOR CONTRIBUTIONS

Conceptualization, L.-F.C., N.E.B., and A.E.W.; Methodology, L.-F.C., M.G.-S., and Y.T.L.; Software, M.G.-S. and Y.T.L.; Formal Analysis, L.-F.C. and Y.T.L.; Investigation, L.-F.C., M.F.H., D.A.G., M.G.Y., B.K., and A.S.Z.; Resources, L.H.; Writing – Original Draft, L.-F.C. and A.E.W.; Writing – Review &Editing, all authors; Visualization, L.-F.C., M.G.-S., and Y.T.L.; Supervision, J.G., C.A.G., N.E.B., and A.E.W.; Funding Acquisition, J.G., C.A.G., N.E.B., and A.E.W.

DECLARATION OF INTERESTS

C.A.G. is a cofounder of and scientific adviser to Element Genomics and Locus Biosciences and is an adviser to Sarepta Therapeutics. C.A.G. and L.H. have submitted patent applications related to epigenome editing.

SUPPLEMENTAL INFORMATION

Supplemental Information includes seven figures and five tables and can be found with this article online at https://doi.org/10.1016/j.celrep.2019.01.032.

transcription by prolonging burst duration and resulted in higher Fos protein levels and an elevation of resting membrane potential. Inhibiting histone acetylation reduced *Fos* transcription by reducing burst frequency and impaired experience-dependent Fos protein induction in the hippocampus *in vivo*. Thus, activity-inducible histone acetylation tunes the transcriptional dynamics of experience-regulated genes to affect selective changes in neuronal gene expression and cellular function.

In Brief

Using CRISPR-mediated epigenome editing, Chen et al. show that enhancer histone acetylation fine-tunes the activity-dependent transcription of *Fos* in neurons.

Graphical Abstract

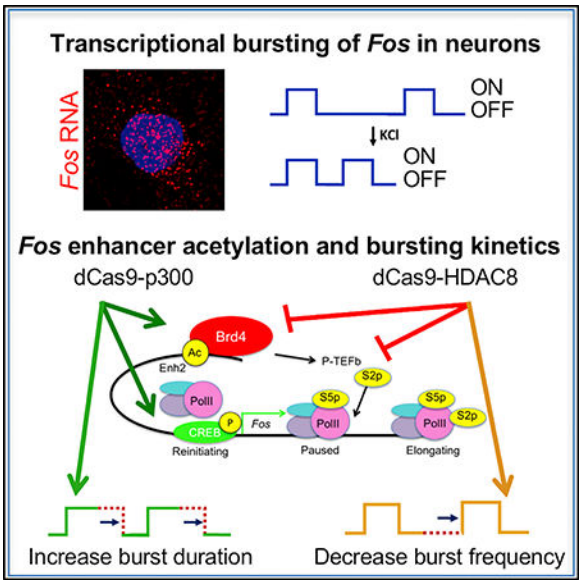

INTRODUCTION

Transient sensory experiences are transduced into long-lasting changes in synaptic connectivity and neuronal function through the activity-dependent regulation of new gene transcription (Chen et al., 2017). Synaptic activity regulates gene transcription by activating intracellular calcium-dependent signaling cascades that modify the function and/or expression of activity-dependent DNA-binding transcription factors and chromatin regulatory proteins (Greer and Greenberg, 2008). The targets of these activity-regulated signaling pathways in neurons include both immediate-early gene transcription factors and neural-specific programs of gene expression, which directly alter aspects of neuron and synapse structure and function (Leslie and Nedivi, 2011). In this manner, stimulus-induced transcription provides a compelling mechanism of activity-dependent neuronal plasticity.

Genome-level sequencing studies have revealed important roles for chromatin state and structure in the control of gene transcription. In addition to gene promoters, distal enhancers contribute to the activation of gene transcription because of conformational loops that bring

them physically close to gene promoters (Heintzman et al., 2009). Enhancers are characterized by their accessibility to transcription factor binding, as well as their enrichment for specific epigenomic marks, including methylation (me) and acetylation (ac) on specific histone H3 lysine (K) residues (H3K4me1 and H3K27ac). Enhancers have been best studied for their role in controlling cell-type-specific programs of gene expression, for which the differential recruitment of the histone acetyltransferases p300 and CREB binding protein (CBP), as well as the presence of H3K27ac, are strong predictors of regulatory elements that are sufficient to drive cell-type-specific gene transcription (Blow et al., 2010; Nord et al., 2013; Visel et al., 2013). However, neurons undergo dynamic changes in their gene expression repertoires long after they have committed to a postmitotic identity; thus, neurons serve as an ideal substrate for studying the biological functions of the epigenome beyond its role in establishing cellular identity. Membrane depolarization of embryonic mouse cortical neurons induces CBP binding and H3K27ac at a subset of putative enhancers near activity-regulated genes, and regulatory elements that show activity-dependent increases in H3K27ac are highly likely to be sufficient to drive activity-dependent transcription of a reporter gene (Kim et al., 2010; Malik et al., 2014). Yet despite widespread correlations between histone modifications and enhancer function, whether these modifications play causative roles in enhancer activity is not always clear (Dorighi et al., 2017). Furthermore, although biochemical studies have shown steady-state increases in both H3K27ac and mRNA at specific time points following neuronal activation, the temporal relationship between these two events is poorly understood.

Transcription is an inherently stochastic process determined by the kinetics of the biochemical events that mediate the synthesis of RNA (Symmons and Raj, 2016). As a consequence, the transcription of most genes when observed at the single-cell level stochastically occurs at a higher rate during long intervals of time called transcriptional bursts, followed by variable periods of transcriptional inactivity (Dar et al., 2012). Bursting can be described by the frequency, duration, and size of the active intervals, which reflect dynamic promoter transitions between inactive and active states. Burst kinetics are highly gene specific and tuned by the diverse array of molecular regulatory mechanisms that control transcription (Suter et al., 2011). Transcription factor binding, enhancer function, and chromatin features have all been linked to effects on burst kinetics in a context-specific manner (Fukaya et al., 2016; Wu et al., 2017). Emerging evidence also suggests that dynamic changes in chromatin state can modulate burst properties to control gene expression levels. For example, inducible histone acetylation at gene promoters covaries with increased burst frequency across the circadian cycle for several mammalian circadian genes (Nicolas et al., 2018).

CRISPR-based methods have emerged as a powerful tool for studying the functions of chromatin regulation, because the site specificity of Cas9 binding, together with its ability to be fused to enzymatic domains, permits the isolated experimental manipulation of histone and DNA modifications at specific sites across the genome (Thakore et al., 2016). Here, to discover how neuronal activity-induced enhancer histone acetylation regulates the transcription of neuronal activity-inducible genes, we first applied quantitative single-molecule fluorescence *in situ* hybridization (smFISH) to establish transcriptional burst kinetics of the neuronal activity-inducible *Fos* and *Npas4* genes in primary neurons in

culture and *in vivo* and then used CRISPR-based dead Cas9 (dCas9) epigenome editing to locally mimic or block activity-induced histone acetylation at well-established enhancers of these genes. Our data show how enhancer histone acetylation modulates the burst dynamics of activity-inducible genes and demonstrate that the regulation of *Fos* bursting is transmitted to regulate Fos protein levels and functional properties of neurons.

RESULTS

Transient Membrane Depolarization Drives Dynamic H3K27ac at Fos Regulatory Elements in Neurons

Membrane depolarization mediated by the elevation of extracellular potassium chloride (KCl) levels is a robust stimulus for the induction of neuronal activity-regulated genes, acting via well-established intracellular calcium signal transduction mechanisms and known to induce histone acetylation of activity-regulated enhancers and promoters (Bito et al., 1996; Halder et al., 2016; Lyons and West, 2011; Malik et al., 2014). The signaling steps that comprise this process, as well as *Fos* mRNA induction and subsequent degradation, occur on the time course of seconds to minutes (Bito et al., 1996; Dolmetsch et al., 2001; Zhai et al., 2013). However, most prior studies of membrane depolarization-inducible H3K27ac have used persistent or hours-long stimulation paradigms (Kim et al., 2010; Malik et al., 2014; Tyssowski et al., 2018). Thus, here we chose to use a minimal stimulation paradigm to ask whether histone acetylation is dynamically regulated on the same timescale as gene transcription.

We stimulated dissociated embryonic mouse cortical neurons in culture with a 5 min pulse of membrane depolarization by elevating extracellular KCl to 55 mM (Lyons et al., 2016). We then measured levels of Fos mRNA by qPCR and H3K27ac by chromatin immunoprecipitation (ChIP) at regulatory elements of the *Fos* gene (Figure 1A) as a function of time after the stimulus was removed. 5 min of membrane depolarization was sufficient to drive stimulus-dependent increases in both *Fos* mRNA and H3K27ac at the *Fos* promoter and distal enhancers (Figure 1B). Induction of *Fos* mRNA, as well as H3K27ac, in response to this stimulus was both rapid and transient, significantly increasing within 10 min following stimulus induction and falling back to basal levels within an hour after cessation of the stimulus (Figure 1B). These data establish a system in which we can study the dynamics of neuronal activity-inducible gene transcription and H3K27a. Furthermore, these data establish the coincident regulation of H3K27ac at *Fos* regulatory elements during the time course of active *Fos* transcription.

Single-Neuron Analysis of Fos and Npas4 mRNA Expression Reveals Dynamics of Transcriptional Bursts

Transcriptional bursts occur whenever a promoter transitions from an inactive to an active state. However, because the biochemical events that mediate these bursts are stochastic, bursts fluctuate randomly over time such that only a subset of cells in a population will be bursting at any given moment (Symmons and Raj, 2016). It is possible to use mathematical models of stochastic gene expression to infer dynamic properties of transcriptional bursting

from the measured distribution of RNA expression in cells sampled from a population (Gómez-Schiavon et al., 2017; Vera et al., 2016).

To determine the burst dynamics of activity-dependent genes in neurons, we first quantified *Fos* mRNA at the single-neuron level in cultured embryonic mouse hippocampal neurons by smFISH (Raj et al., 2008). We fixed cells for smFISH both under basal conditions (in the presence of tetrodotoxin [TTX]) and at various times following a brief period (as in Figure 1B) of membrane depolarization (Figure 2A). The distributions of fluorescence intensities of cytoplasmic mRNA spots fit a Gaussian distribution, consistent with each spot representing a single mRNA molecule (Figures S1A and S1B). The time course and magnitude of the average number of mRNAs detected per neuron by smFISH across all cells in the population precisely paralleled the changes we observed for the same stimulus and time course using qPCR, validating the measure (Figure 2B). Because multiple nascent RNAs from stimulus-induced genes accumulate near the transcription site (TS) in the nucleus before splicing and export (Bhatt et al., 2012; Senecal et al., 2014), smFISH also reveals the total number of active TSs (0, 1, or 2) for each gene within each neuron that are actively being transcribed at any given time point, providing a key measure of promoter state at each allele in a given cell (Figures 2A and 2C). Colocalization of smFISH signal for *Fos* introns with the nuclear *Fos* exon signal confirmed that these nuclear clusters are composed of nascent RNA (Figure 2C). We performed parallel measurements for the neuronal activity-regulated gene *Npas4* in an independent set of neurons (Figures 2A and S1C) (Gómez-Schiavon et al., 2017).

In the presence of TTX, both *Fos* and *Npas4* mRNA levels were low but detectable in most neurons, with a distribution of cytoplasmic mRNA levels and either 0 or 1 active TSs detected per cell (Figures 2D and S1D). Following membrane depolarization, the mean levels of mRNAs were elevated over time (Figures 2D and S1D). However, there was increased variability in the distributions of mRNA between cells, and although the proportion of neurons showing both active alleles (TS = 2) for *Fos* or *Npas4* increased following membrane depolarization and reached a peak 10 min following cessation of the stimulus (Figures 2D and S1D), we observed a substantial fraction of neurons that had only 0 or 1 active alleles. When we compared the levels of Fos protein in single neurons induced by the same pulse of membrane depolarization, we found wide variation in Fos protein levels when comparing single cells in the population. This strongly suggests that the transcriptional variation in *Fos* mRNA induction propagates and contributes to differences in the levels of Fos protein between neurons (Figure 2E).

The cell-to-cell and allele-to-allele variability in RNA expression that we observed in neurons is consistent with the hypothesis that these genes are transcribed in stochastic bursts in neurons both under basal conditions and following transcriptional induction by membrane depolarization. To quantify these dynamic transcriptional properties and to understand how they change upon neuronal activation, we used a computational pipeline (BayFish) (Gómez-Schiavon et al., 2017) to infer kinetic parameters of transcription and promoter-state transitions from the measured distributions of mRNA and active alleles (Figure 2D) at time points before stimulation (basal) and after stimulation (5 min KCl + 0 min, 10 min, or 20 min).

Parameter inference using BayFish derives from an underlying mathematical model of gene transcription and promoter states. We considered the simplest model of transcriptional bursting (known as a two-state promoter model), in which the promoter of each allele can be either active (ON) or inactive (OFF) (Figure 2F). Our two-state model has a minimum of five kinetic parameters to be inferred: the rate at which each promoter turns on (k_{ON}), the rate at which each promoter turns off (k_{OFF}), the RNA synthesis rate for each ON promoter (μ) and for each OFF promoter (μ_0), and a delay (τ) between transcription initiation and production of mature, cytoplasmic mRNAs. The rate of *Fos* RNA degradation (δ) was measured previously (Shyu et al., 1989) and kept constant in our model. However, upon membrane depolarization, one or more of the kinetic parameters could change to cause increased levels of transcription. Previously, we showed for *Npas4* that increasing the promoter activation rate (from k^U_{ON} to stimulated k^S_{ON}) upon membrane depolarization had the best and most parsimonious fit to the smFISH data when compared to other models of induction (Gómez-Schiavon et al., 2017). Thus, we applied the same induction model to both *Fos* and *Npas4* smFISH data to infer kinetic parameters using BayFish (Figures S1E and S1F; Table S1). Inferred rates of promoter-state transitions were comparable to or slower than the timescale of transcript elongation and maturation (τ of ~3 min). The average length of time each promoter spent in the ON state was ~11 min, whereas the average duration of the OFF state changed from ~100 to ~4 min upon membrane depolarization, thus increasing the fraction of time spent in the ON state (Figure 2G). These data indicate that the measured cell-to-cell variations in the levels of *Fos* and *Npas4* mRNA likely arise from transcriptional bursting due to slow promoter-state transitions and that induction increases the probability *Fos* or *Npas4* promoter transitions to the ON state, thus increasing burst frequency, in agreement with previous work (Gómez-Schiavon et al., 2017; Senecal et al., 2014).

Intrinsic Variability in the Probabilistic Activation of Fos and Npas4 Gene Promoters in Single Neurons

The variability in *Fos* and *Npas4* mRNA expression between neurons could arise from differences in the capacity of individual neurons to receive or propagate calcium-dependent signaling events to the nucleus (extrinsic variability), or it could arise from gene-local chromatin features that influence the probabilistic activation of gene promoters (intrinsic variability). Several pieces of data pointed toward an important role for gene-intrinsic determinants of transcriptional activation in our neurons. First, our hippocampal cultures are relatively homogeneous populations of excitatory neurons (Figure S2A). Second, all neurons responded to membrane depolarization with a robust increase in intracellular calcium concentration (Figure S2B). Finally, when we varied the extracellular calcium concentration in the medium, we found that although the accumulation of *Fos* RNA at the TSs depends on a minimum calcium concentration, the number of active *Fos* TSs did not increase further when extracellular calcium rose above this threshold (Figure S2C). At all concentrations of calcium tested, we still found a substantial number of neurons with only 1 TS active, although both TSs in a single cell have exposure to the same upstream calcium signaling events.

To provide a direct comparison of intrinsic versus extrinsic variability at the single-cell level, we reasoned that if there is substantial cell-to-cell variation in the activation of calcium-

dependent transcriptional signaling pathways in our population, we should see concordant activation of multiple activity-dependent genes in any single neuron. Alternatively, if the variability we observe for any single gene mostly arises from probabilistic activation intrinsic to the gene promoter, then we should see uncoordinated induction of multiple activity-dependent genes in a single neuron.

To examine transcriptional concordance in single neurons, we simultaneously quantified mRNA for *Fos* and *Npas4* in single hippocampal neurons by two-color smFISH following membrane depolarization in culture (Figure 3A). Even though *Fos* and *Npas4* have similar kinetics and magnitude of induction at the population level (Figures 2B and S1C), we found a relatively weak correlation between the depolarization-induced levels of these two mRNAs in single neurons (Figure 3B). Our data also reveal variability in the transcriptional activation of each of the two *Fos* and *Npas4* alleles within a single neuron (Figure 3C). Although many neurons in our population transitioned from having both alleles of *Fos* and *Npas4* off (0,0) to having both alleles on (2,2) following membrane depolarization, at each time point, we also found substantial numbers of neurons in which only a single allele of one gene was active in various combinations with 0, 1, or 2 active alleles of the other gene.

To assess whether intrinsic determination of promoter activation also occurs in adult neurons in response to physiologically relevant environmental stimuli *in vivo*, we performed dual-color *Fos* and *Npas4* smFISH on sections from visual cortex of dark-adapted mice before and after light exposure (Figure 3D). Because *Npas4* is a neural-selective gene, whereas *Fos* is also inducible in non-neuronal cells, we first identified *Npas4*-positive neurons in the visual cortex and then quantified the number of active *Npas4* and *Fos* alleles in the nuclei of these neurons (Figures 3E and 3F). Few cells had detectable *Npas4* mRNA in the visual cortex of dark-adapted mice, and all of these had no detectable active TSs for *Fos* (Figure 3G). Consistent with previous studies (Hrvatin et al., 2018), light exposure led to a robust induction of *Npas4* and *Fos* mRNA in visual cortex, as measured both by a significant increase in the number of *Npas4*-positive neurons and by the appearance of nascent RNA accumulation at activated TSs for both *Fos* and *Npas4* in the nuclei of these neurons (Figures 3F and 3G). However, when we compared both genes at the single-neuron level, we again found many cells with activation of only a subset of the 2 *Fos* and 2 *Npas4* alleles, indicating gene intrinsic regulation of the probability of *Fos* and *Npas4* promoter activation in neurons *in vivo*.

Bidirectional CRISPR-Mediated Editing of Histone Acetylation at Gene Regulatory Elements by dCas9-p300 and dCas9-HDAC8

We next sought to determine whether local H3K27ac accumulation at enhancers contributes to transcriptional kinetics of these genes. To directly modulate H3K27ac at specific gene regulatory elements, we used CRISPR-based methods to locally tether enzymatically dCas9 fusion proteins to either the *Fos* promoter or the putative activity-regulated enhancers of the *Fos* and *Npas4* genes (Kim et al., 2010) (Figures 1A, S3A, and S4A). We compared the effects on mRNA expression of enhancing local histone acetylation through recruitment of the histone acetyltransferase (HAT) dCas9-p300 (Hilton et al., 2015) to the effects of

reducing local histone acetylation through recruitment of the histone deacetylase (HDAC) dCas9-HDAC8.

We observed a significant increase of *Fos* mRNA in dCas9-p300-transfected N2A cells cotransfected with guide RNAs (gRNAs) targeting the *Fos* promoter compared with control gRNA cotransfected cells (Figure 4A). We also observed a significant increase of *Fos* mRNA expression over control in cells transfected with dCas9-p300 and gRNAs targeting *Fos* enhancer (Enh) 1, Enh2, Enh4, or Enh5, but not Enh3 (Figure 4A). The induction of *Fos* was due to dCas9-p300 recruitment to *Fos* enhancers and is not a non-specific effect on N2A cell physiology, because expression of another *Fos* family member, *Fosb*, and *Npas4* was unaffected in cells cotransfected with dCas9-p300 and *Fos* Enh2 gRNAs compared to control (Figure S3C). Thus, of the five putative enhancers near *Fos* that were initially identified by their inducible CBP binding and H3K27ac accumulation following neuronal membrane depolarization (Kim et al., 2010; Malik et al., 2014), only four are either necessary (Joo et al., 2016) or sufficient (Figure 4A) for *Fos* transcriptional regulation. We similarly tested two putative CBP/ H3K27ac+ enhancers upstream of the *Npas4* gene and identified one for which dCas9-p300 recruitment significantly increased *Npas4* mRNA expression (Figures S4A and S4B).

To verify the mechanisms by which the dCas9-p300 fusion protein promotes transcription, we focused on acetylation of *Fos* Enh2. Each of the four verified *Fos* enhancers shows specificity for activation by different upstream stimuli, and Enh2 is the most responsive to neuronal membrane depolarization through the elevation of extracellular KCl (Joo et al., 2016). To test whether HAT activity of the dCas9-p300 fusion protein is required for Enh2-mediated *Fos* transcription, we used a mutant dCas9-p300 fusion protein bearing a single amino acid mutation (D1399Y; dCas9-p300DY) in the enzymatic domain of p300 that eliminates its HAT activity (Hilton et al., 2015). All dCas9 fusions were expressed at similar levels in N2A cells (Figure S3D). Whereas cells cotransfected with the HAT-active dCas9 fusion protein and the gRNAs targeting Enh2 induce *Fos* expression, cells cotransfected with the HAT mutant dCas9 fusion protein failed to induce *Fos* expression (Figure 4B). ChIP using an antibody against a FLAG epitope on the dCas9 fusion proteins showed that both dCas9-p300 and dCas9-p300DY were recruited to *Fos* Enh2 by the Enh2 gRNAs (Figure 4C). This binding was specific to Enh2, because there was no significant interaction of either dCas9 fusion protein at the *Fos* promoter or other *Fos* enhancers (Figures 4C and S3E). To confirm that CRISPR-targeted dCas9-p300 locally increases H3K27ac at targeted enhancers, we performed ChIP to measure H3K27ac at the *Fos* promoter and enhancers in transfected cells. Compared with control, we observed significantly higher H3K27ac at *Fos* Enh2 in cells cotransfected with dCas9-p300 and Enh2 gRNAs, whereas cotransfection of Enh2 gRNAs with the HAT-dead dCas9-p300DY construct did not increase H3K27ac over control levels (Figure 4D). This increase in H3K27ac was local to the enhancer where the dCas9-p300 fusion protein was recruited, and we saw no increase of H3K27ac at the *Fos* promoter and other enhancers (Figures 4D and S3F).

To determine the effects of reducing histone acetylation on stimulus-inducible *Fos* transcription, we performed parallel experiments using CRISPR-mediated recruitment dCas9-HDAC8 fusion protein to *Fos* Enh2. Recruitment of dCas9-HDAC8 to *Fos* Enh2

(Figures 4E and S3G) reduced H3K27ac locally at Enh2 compared with N2A cells expressing dCas9-HDAC8 and a control gRNA but had no significant effect on acetylation of the *Fos* promoter and other enhancers (Figures 4F and S3H). Consistent with a requirement for stimulus-induced enhancer histone acetylation in transcriptional activation of the *Fos* gene, recruitment of dCas9-HDAC8 to *Fos* Enh2 impaired forskolin-dependent induction of *Fos* in N2A cells but had no effect on expression under basal conditions (Figure 4G). This effect was not a non-specific effect on N2A cell physiology, because forskolin induction of *Dusp1* was unaffected in cells cotransfected with dCas9-HDAC8 and *Fos* Enh2 gRNAs compared to control (Figure S3I).

Local Regulation of H3K27ac at Enhancers Modulates Transcriptional Burst Dynamics in Neurons

We next cotransfected primary mouse hippocampal neurons with dCas9-p300 and either a control gRNA or a pool of gRNAs targeting Enh2 and quantified the number of *Fos* mRNAs per cell and the number of active TSs by smFISH before and at time points after a 5 min period of membrane depolarization (Figure 5A). Recruitment of dCas9-p300 selectively to *Fos* Enh2 significantly increased *Fos* mRNA expression in neurons both under basal conditions and following membrane depolarization (Figure 5B), similar to the effects of the HDAC inhibitor TSA (Figure S5). In parallel experiments, we observed an increase in RNA expression when we recruited dCas9-p300 to the upstream enhancer of *Npas4*, although the enhancement was significant only following membrane depolarization-induced transcription of *Npas4* (Figure S4D). To determine whether the endogenous induction of H3K27ac at gene enhancers that is induced by membrane depolarization (Figure 1B) is required for the transcriptional response to this stimulus, we cotransfected hippocampal neurons with gRNAs and dCas9-HDAC8 to reduce H3K27ac at Enh2. Recruitment of dCas9-HDAC8 to *Fos* Enh2 significantly decreased *Fos* mRNA expression in neurons both under basal conditions and following membrane depolarization (Figure 5C).

Having established bidirectional regulation of *Fos* transcription with complementary manipulations of H3K27ac at *Fos* Enh2, we used BayFish to infer how the kinetic parameters of promoter-state transitions changed as a result of these manipulations. We again implemented the two-state model shown in Figure 2F and inferred the best-fit parameters for dCas9-p300-or dCas9-HDAC8-transfected neurons, comparing control versus Enh2 gRNA transfected for each pair. The marginal posterior distributions for the ON rates (basal and stimulated), OFF rate, synthesis rates (basal and stimulated), and delay term are shown in Figure S6.

Our results indicate that recruiting dCas9-p300 (+ac) to *Fos* Enh2 predominantly reduced the OFF rate relative to control-transfected neurons (Figure 5D; Table S2), prolonging the time that the promoter stays in the active state after it turns on and thus increasing burst duration. Because dCas9-p300 mimics the activity-inducible gain of H3K27ac at Enh2, these data suggest that the dynamic loss of H3K27ac from gene enhancers following membrane depolarization (Figure 1B) contributes to shaping the kinetics of *Fos* transcription by limiting burst length. By contrast, our results indicate that recruiting dCas9-HDAC8 (-ac) to *Fos* Enh2 predominantly reduces the ON rate relative to control-transfected neurons. The

effect of decreasing the ON rate is that promoters spend a longer time in the OFF state, which decreases the overall frequency of bursts (Figure 5E; Table S2). These data suggest that the endogenous histone acetylation induced by membrane depolarization at enhancers is shaping the dynamic transcriptional response to this stimulation by contributing to the increased frequency of bursting seen upon stimulation. These inferences of the model are consistent with our evidence for altered *Fos* RNA expression upon manipulation of enhancer H3K27ac under both basal and stimulus-induced conditions. However, because bursting is more frequent following membrane depolarization, the effect of either manipulation will be greatest following stimulus-inducible transcriptional activation.

Enhancer Acetylation Recruits Brd4 to Promote Transcriptional Elongation

Acetylated lysines serve as docking sites for bromodomain-containing proteins such as Brd4, which acts as a master regulator of transcriptional elongation (Winter et al., 2017). Brd4 has been shown to mediate stimulus-dependent activation of transcriptional elongation when recruited to enhancers in non-neuronal cells (Zippo et al., 2009), and it has been proposed to contribute to activity-dependent transcription in neurons (Korb et al., 2015). Brd4 regulates elongation by recruiting the P-TEFb complex, which triggers RNA polymerase II (Pol II) phosphorylation on Ser2 and promotes highly rapid and productive transcriptional elongation of paused genes (Jonkers and Lis, 2015). *Fos* and *Npas4* belong to a large set of neuronal activity-regulated genes whose promoters are occupied under basal conditions by Pol II complexes that are initiated but stably paused in neurons (Saha et al., 2011). Thus, we asked whether enhancer histone acetylation regulates *Fos* transcription via its ability to recruit Brd4 and promote transcriptional elongation.

Consistent with a role for Brd4 in enhancer acetylation-dependent activation of *Fos*, we observed significantly more Brd4 binding by ChIP at Fos Enh2, but not the *Fos* promoter, in N2A cells when dCas9-p300 was recruited to this enhancer compared with control (Figure 6A). The recruitment of Brd4 is required to couple dCas9-p300 recruitment at Enh2 to enhance *Fos* transcription, because treatment of N2A cells with the bromodomain inhibitor JQ1, which competitively blocks binding of Brd4 to acetylated histones, blocked the ability of dCas9-p300 recruited to Enh2 to increase *Fos* mRNA expression (Figure 6B). The increase in Brd4 binding at Enh2 driven by dCas9-p300 recruitment was associated with increased *Fos* transcriptional elongation, because the level of Ser2-phosphorylated Pol II (pSer2-RNAPII) was significantly elevated on the *Fos* gene in cells cotransfected with dCas9-p300 and Enh2 gRNAs compared to control. Furthermore pSer2-RNAPII was elevated at both the 5’ and the 3’ ends of the *Fos* gene in these cells, indicating that acetylation of enhancer 2 was sufficient to induce productive increases in Pol II elongation across the length of the *Fos* gene (Figure 6C). By contrast, ChIP with an antibody (8WG16) that preferentially recognizes the non-phosphorylated version of Pol II (Jones et al., 2004) showed a significant reduction at the *Fos* promoter in cells cotransfected with dCas9-p300 and Enh2 gRNAs compared to control (Figure 6D), suggesting that the increase in elongating pSer2-RNAPII was due to an activation of paused Pol II complexes rather than an overall increase in Pol II recruitment.

Changes in Enhancer Histone Acetylation Mediate Physiologically Relevant Differences in Fos Protein Expression and Function in Neurons

To determine whether activity-dependent regulation of histone acetylation at *Fos* enhancers has relevance for plasticity of neuronal function, we first asked whether the induction of *Fos* transcription achieved by targeting dCas9-p300 to Enh2 was sufficient to drive changes in Fos protein expression and function. We observed a significant increase of Fos protein levels in neurons transfected with *Fos* Enh2 gRNAs compared with control gRNA-transfected neurons, indicating that the increased *Fos* mRNA we observed in these neurons was translated into increases in Fos protein (Figures 7A and 7B). Because Fos is a transcription factor, once its expression is induced, Fos binds AP-1 elements across the genome to regulate the expression of secondary response genes in a cell-type-specific manner. In N2A cells cotransfected with a 3xAP-1 firefly luciferase reporter plasmid and dCas9-p300, cells transfected with *Fos* Enh2 gRNAs had significantly more firefly luciferase (*FLuc*) mRNA compared to control-transfected cells (Figure 7C). These data show that the activation of *Fos* transcription induced by enhancer histone acetylation is sufficient to increase Fos-dependent transcription; however, the cellular consequences of that increase will depend on the cell-type-specific targets of Fos-dependent regulation. Although the precise cell-autonomous consequences of Fos induction in hippocampal neurons remain to be determined, elevated Fos levels affect the expression of ion channels (Su et al., 2017) that could change the membrane properties of hippocampal neurons. Consistent with this possibility, and similar to the effects of *Fos* overexpression (Figures S7A and S7B) or *in vivo* Fos induction (Whitaker et al., 2017), we found that hippocampal neurons cotransfected with dCas9-p300 and Enh2 gRNAs showed significantly higher resting membrane potentials compared with control-transfected neurons (Figure 7D).

Finally, to determine whether stimulus-inducible regulation of enhancer acetylation of *Fos* regulatory elements contributes to the induction of *Fos* expression in adult neurons *in vivo* in response to sensory stimulation, we generated lentiviral vectors coexpressing dCas9-HDAC8 and either a control gRNA or a single gRNA targeting Fos Enh2 (Figures S3A and S3B) (Enh2 gRNA1) and delivered these viruses by stereotaxic injection into the dorsal hippocampus of adult mice (Figure 7E). Mice were exposed to a novel environment, which promotes robust induction of Fos expression in neurons throughout the hippocampal formation (VanElzakker et al., 2008). Similar to other studies (Jaeger et al., 2018), we detected Fos protein after exposure in neurons in the dentate gyrus (DG), with a bimodal distribution of expression levels that we classified as low Fos+ and high Fos+ neurons (Figures S7C and S7D). We found similar numbers of dCas9-HDAC8-positive cells in the DG on the control and *Fos* Enh2 virus-infected sides of the brains (control [Ctrl] = 62.25 ± 17.5, Enh2 = 49.86 ± 13.18, n = 7 Ctrl, 8 Enh2 hemispheres/virus, p = 0.59), and consistent with the relatively sparse infection induced by lentiviruses *in vivo* (Figure 7F), we saw no significant side-to-side difference in the average total number of high Fos+ cells (Ctrl = 43.25 ± 9.82, Enh2 = 24.71 ± 7.2, p = 0.16). However, when we quantified Fos expression only in the dCas9-HDAC8-positive neurons, we found that a significantly smaller percentage of the Fos+ cells expressing the dCas9-Hdac8/Enh2 virus showed expression in the high Fos + range compared with dCas9-HDAC8-expressing cells from the Ctrl virus side of the brain (Figure 7G) (Ctrl = 8.08% ± 2.11%, Enh2 = 2.32% ± 0.93%, p = 0.03). These data show that

local inhibition of enhancer histone acetylation is sufficient to impair stimulus-inducible Fos expression in response to environmental stimuli in the hippocampus *in vivo*.

DISCUSSION

Epigenome profiling studies have shown the distribution of chromatin marks across the genome and their correlative relationship to gene expression. These data have driven the formation of hypotheses of the functional consequences of chromatin regulation, including the possibility that the priming of histone modifications or DNA methylation at regulatory elements controlling stimulus-regulated genes could modulate behavioral responses to the environment (Gräff and Tsai, 2013). Epigenome editing offers an opportunity to test the causative role of chromatin modifications for gene transcription via the local recruitment of histone-modifying enzymes to specific gene regulatory elements (Thakore et al., 2016). We have used this methodology to study the transcriptional consequences of histone acetylation at enhancers of the neuronal activity-inducible gene *Fos*. Our data reveal mechanistic insights into how this enhancer modification changes the dynamics of activity-inducible gene transcription.

Transcription is a probabilistic process, such that many genes are transcribed in a pulsatile fashion, with temporally regulated bursts of new transcription staggered in time at the single-cell level. Prior single-cell studies of steroid- and serum-inducible genes have indicated that the increases in RNA expression that follow cellular stimulation arise due to an increase in the frequency or the duration of bursts (Larson et al., 2013; Molina et al., 2013; Senecal et al., 2014). Our single-neuron smFISH data for *Fos* and *Npas4* (Gómez-Schiavon et al., 2017) are well fit by a bursting model in which membrane depolarization decreases the time until a given promoter transitions to the ON state, which results in more frequent bursts (Figure 2G). This model matches with the known molecular mechanisms used by calcium-dependent intracellular signal pathways to turn on gene expression, in which the phosphorylation of transcription factors enhances recruitment of the transcriptional machinery to activity-inducible gene promoters, mediating their activation (Lyons and West, 2011). Consistent with our data, a study used engineered RNA tags to perform live imaging of transcription from the *Arc* gene in neurons, and this revealed stimulus-dependent regulation of transcriptional bursts (Das et al., 2018). To induce *Arc*, the authors used TTX withdrawal, which activates both synaptic NMDA receptor and L-type voltage-sensitive calcium channel (VSCC)-dependent gene transcription (Ghiretti et al., 2014). This stimulus induced *Arc* by prolonging burst duration, rather than by changing burst frequency (Das et al., 2018). Testing whether the differences in burst dynamics observed between this study and ours arise from the genes studied or the stimuli used will be a useful means to discover molecular mechanisms that determine burst properties in neurons. Finally, although the timescale (order of minutes) of the stimulus we used in this study was commensurate with the burst kinetics we observed, it would be valuable in the future to examine the burst kinetics of activity-dependent gene induction following temporally complex patterned stimuli like those known to induce synaptic plasticity. Differences in the induction of neuronal activity-regulated genes have been linked to distinct patterns (Lee et al., 2017) or the duration (Tyssowski et al., 2018) of upstream stimuli, and using bursting

kinetics offers a quantitative way to more precisely define the input-output relationship between neuronal activity and transcriptional induction of plasticity genes.

Enhancers serve as binding sites for transcription factors, and as such, they regulate gene promoters by increasing the local likelihood of the intermolecular interactions that underlie the formation of active transcriptional regulatory complexes (Levine et al., 2014). However, modified histones can also serve as docking sites for transcriptional regulatory proteins, suggesting a potential causative mechanism by which these chromatin marks can affect transcriptional processes (Winter et al., 2017). The challenge for testing the functional importance of protein interactions with histones has been finding a way to isolate the modification of histones at regulatory elements independent of the changes in transcription factor binding and/or activation that normally accompany the induction of these modifications. Here we achieve that goal by using CRISPR-dCas9 to engineer increased histone acetylation at *Fos* enhancers. In the context of neuronal activity-induced *Fos* transcription, our model suggests that the induction of enhancer histone acetylation contributes to the ability of neuronal activity to transition the *Fos* promoter to the “on” state, because blocking this induction with dCas9-HDAC8 recruitment to Enh2 reduces burst frequency (Figure 5E). However, our data also suggest that the dynamic loss of H3K27ac at *Fos* enhancers facilitates the transition of the Fos promoter to the OFF state, because recruiting dCas9-p300 to Enh2 to persistently increase enhancer acetylation prolonged burst duration (Figure 5D).

Our data show that enhancer acetylation-dependent recruitment of Brd4 promotes the transcriptional elongation of *Fos*, which requires the release of paused Pol II. Release of Pol II pausing is required for the rapid activity-dependent induction of a large set of genes, including *Fos* and *Npas4*, following synaptic activation (Saha et al., 2011). These data suggest that dCas9-HDAC8 recruitment to *Fos* Enh2 decreases burst frequency by impairing the transition of paused Pol II to the actively elongating form. It is also possible that persistent Brd4 recruitment to Enh2 by dCas9-p300 increases burst duration through a similar mechanism. Transcriptional bursts are characterized by the rapid successive initiation of multiple Pol II complexes at gene promoters (Larson et al., 2011), yet paused Pol II has been shown to inhibit new transcriptional initiation at genes (Shao and Zeitlinger, 2017). If these two processes are in dynamic equilibrium, then prolonged relief of pausing could favor additional rounds of initiation, lengthening the duration of transcriptional bursts. Small-molecule inhibition of Brd4 binding with JQ1 *in vivo* has been shown both to blunt stimulus-dependent induction of genes, including *Fos*, and to impair behavioral performance in memory tasks (Korb et al., 2015), suggesting the functional relevance of Brd4-dependent transcriptional elongation for neuronal plasticity.

Our bursting data show how chromatin regulators fine-tune the dynamic features of stimulus-inducible gene transcription. Just as importantly, our data show that dCas9-CRISPR-mediated modulation of histone acetylation at enhancers of *Fos* and *Npas4* does not override the activity dependence of the transcription of these genes. Specifically, membrane depolarization still increases burst frequency, regardless of the acetylation state of the *Fos* regulatory enhancer we targeted. This preservation of stimulus-dependent regulation is distinct from other published strategies for dCas9 or zinc-finger nuclease-mediated

activation (e.g., VP64 and p65) or inhibition (e.g., Krab and G9a), which predominantly enable constitutive activation or repression of target genes (Heller et al., 2014; Xu et al., 2018; Zheng et al., 2018; Zhou et al., 2018). These data suggest that modulation of enhancer acetylation using dCas9-p300 and dCas9-HDAC8 could provide a means to test the physiological functions of activity-induced gene expression in neurons. As strategies emerge to allow the application of CRISPR to manipulate the chromatin state *in vivo* (Liu et al., 2016), these tools will present an opportunity to carry the findings revealed here to a circuit level of analysis.

STAR★METHODS

CONTACT FOR REAGENT AND RESOURCE SHARING

Further information and requests for resources and reagents should be directed to and will be fulfilled by the Lead Contact, Anne West (west@neuro.duke.edu).

EXPERIMENTAL MODEL AND SUBJECT DETAILS

Mouse studies—Adult male and female C57BL6/J mice (The Jackson Laboratory) were used for dark/light exposure, with one of each sex used for each experimental condition. Adult male C57Bl6/J mice were used for novel object exploration experiments, and mice were assigned randomly to experimental groups. Timed pregnant CD1 female mice (Charles River Labs) were used for dissociated neuron cultures. Cultures were made from dissociated neurons pooled from all pups in each litter including both males and females. Mice were housed on a 12: 12 h light:dark cycle and given ad lib access to food and water. All experiments were conducted in accordance with an animal protocol approved by the Duke University Institutional Animal Care and Use Committee.

Dissociated primary neuron cultures—Neuron-enriched cultures were generated from cortex or hippocampus as described in the text of male and female E16.5 CD1 mouse embryos (Charles River Laboratories) and cultured as previously described (Lyons et al., 2016). Transfections were performed with Lipofectamine 2000 (Life Technologies) at DIV3–4. Cell were treated with 1 μM Tetrodotoxin (TTX) (Tocris, 1069) 24 hours before membrane depolarization. Isotonic membrane depolarization with 55mM extracellular KCl was done as previously described (Lyons et al., 2016). We used Tyrodes solutions (79mM NaCl, 55mM KCl, 2mM $CaCl_2$, 1mM $MgCl_2$, 30mM Glucose, 25mM HEPES, 0.1% BSA, pH to 7.4) to test the effect of calcium influx on transcriptional activation. When removing calcium, it is necessary to maintain the total concentration of divalent cations (Mg^{2+} and Ca^{2+}) constant at 3mM. Trichostatin A (TSA) (Sigma, T8552) was used at a concentration of 30nM and added 20 hours prior to harvest.

Neuro2a cell culture—*Mus musculus* neuroblastoma Neuro2a (N2A) cells (ATCC #CCL-131) were grown in DMEM with 10% FBS (Hyclone) and 100 units/ml penicillin/ streptomycin. Transfections were performed with Lipofectamine 3000 (Life Technologies) using protocols recommended by the manufacturer. Cells were harvested for analysis 2 day after transfection. Forskolin (Sigma, F3917) were added at 10μM for 30 mins prior to harvest. JQ1 (Sigma, SL1524) were added at 1μM for 24 hours prior to harvest.

METHOD DETAILS

Reverse transcription and quantitative PCR—RNA was harvested using the Absolutely RNA Miniprep Kit (Agilent, 400800) and cDNA was synthesized by Superscript II (Invitrogen, 18064). Quantitative SYBR green PCR was performed on an ABI 7300 real-time PCR machine (Applied Biosystems) using intron-spanning primers (Table S4).

Chromatin Immunoprecipitation-qPCR—Chromatin immunoprecipitation was performed following the protocol of EZ-ChIP (Millipore, 17–371). Briefly, cells were lysed by SDS Lysis Buffer and sonicated for 2 hr (Diagenode Bioruptor) at 4°C on the high setting with 30 s on/off interval. 20 μl Dynabeads Protein G (ThermoFisher, 10003D) was pre-incubated with 2 μg antibodies in ChIP Dilution buffer for 1 hour at 4°C. Cell lysates were then incubated overnight with antibody-bead complexes at 4°C. Subsequently, the beads were washed with Low Salt Immune Complex Wash Buffer, High Salt Immune Complex Wash Buffer, LiCl Immune Complex Wash Buffer and TE Buffer. Bound protein/DNA complexes were eluted by ChIP elution buffer and then reversed the crosslinks. Samples were treated with RNase A and Proteinase K for post-immunoprecipitation and then the DNA was purified using QIAquick PCR Purification Kit (QIAGEN, 28104). H3K27Ac (Abcam, ab4729), Brd4 (Bethyl, A301–985A), Pol II Ser-2P (Abcam, ab5095), POLR2A monoclonal 8WG16 (Thermo Fisher, MA1–26249), and FLAG M2 (Sigma, F3165) antibodies were used. Quantitative SYBR green PCR was performed on an ABI 7300 real-time PCR machine (Applied Biosystems) with primers in Table S5.

Single molecule fluorescence *in situ* hybridization—Neurons were hybridized with Stellaris RNA FISH Probe sets labeled with Quasar 570 or Quasar 670 (Biosearch Technologies, Inc.), following the manufacturer's instructions available online at https://www.biosearchtech.com/support/resources/stellaris-protocols. Briefly, embryonic mouse hippocampal neurons were cultured on PDL/laminin coated glass coverslips (neuVitro) and fixed in 4% paraformaldehyde at room temperature for 10mins. Neurons were then permeabilized overnight by 70% (vol./vol.) ethanol at 4°C. Coverslips were hybridized with 500 nM probes in hybridization buffer (10% Formamide, 10% 20x SSC, 10% Dextran sulfate, 1mg/mL *Escherichia coli* tRNA, 2mM Vanadyl ribonucleoside complex and 20ug/mL BSA) at 37 degree for 4 hours followed by washing and Hoechst staining. For fresh frozen mouse brain, slide-mounted tissue sections were fixed in cold 4% paraformaldehyde for 15mins. Sections were then dehydrated by ethanol and hybridized with 500nM probes in hybridization buffer at 37 degree overnight followed by washing and Hoechst staining. Stellaris® FISH Probes in this study: Mouse Gapdh (Biosearch Technologies, Inc., SMF-3002–1). Custom Stellaris FISH Probe sets were designed against mouse Fos exon, mouse Fos intron and mouse Naps4 exon by utilizing the Stellaris® RNA FISH Probe Designer (Biosearch Technologies, Inc.) available online at https://www.biosearchtech.com/Account/Login?return=/stellaris-designer. Probe sequences are available upon request.

smFISH image acquisition and quantification—Z stack images were captured on either wide-field microscope (DMI4000, Leica) or confocal microscope (TCS SP8, Leica). Wide-field microscope (DMI4000, Leica) equipped with a CCD camera (DFC365 FX,

Leica) and controlled by MetaMorph (Molecular Devices). Objective with NA 1.4 and 63X magnification yielded an xy pixel-size of 146 nm. 35–45 Z-slices were recorded with a 200 nm step-size and 1 s exposure time. Confocal microscope (TCS SP8, Leica) equipped with HyD hybrid detectors (Leica). Objective with NA 1.4 and 100X magnification. The detection field was set at 1024 × 1024 and yielded xy pixel-size of 116 nm. The scan rate was set at 600 Hz and the argon laser was set at 30% intensity. 35–45 Z-slices were recorded with a 200 nm step-size. *Fos* and *Npas4* transcript numbers and active TSs were estimated with FISH-quant (Mueller et al., 2013). Cell body of neurons were segmented manually and active TSs were detected with an intensity threshold (around 1.5 fold of average intensity of single transcript).

Immunofluorescence—Embryonic mouse hippocampal neurons were cultured on PDL/laminin coated glass coverslips (neuVitro, GG-12-laminin) and fixed in 4% paraformaldehyde at room temperature for 10 min. Neurons were blocked in 10% normal goat serum and permeabilized in 0.3% Triton X-100 prior to antibody incubation. Coverslips were incubated in primary antibodies overnight at 4°C. Secondary antibodies were incubated at room temperature for 1 hr. Hoechst dye (0.1μg/ml, Sigma) was used to label nuclei. Primary antibodies used in this study for immunocytochemistry were mouse anti-Fos (EnCor, MCA-2H2, 1:800), mouse anti-GAD65 (Millipore, AB5082, 1:500), and chicken anti-MAP2 (Millipore, AB5543, 1:2000). Images were captured on wide-field microscope (DMI4000, Leica) equipped with a CCD camera (DFC365 FX, Leica) and controlled by MetaMorph (Molecular Devices). For quantification of Fos protein level in primary cultures, images were captured at the best z-plane identified in Hoechst channel and analyzed by Fiji. Transfected neurons were selected based on their GFP signals and then Fos fluorescence intensities were measured in these neurons.

Calcium Imaging—Primary cultured hippocampal neurons plated on glass coverslips were loaded with 2 μM Fura-2 AM (Invitrogen) and 0.04% Pluronic F-127 (Invitrogen) in HANKS buffer (Sigma) at room temperature for 30 min. Cells were imaged every 5 s with an inverted microscope (Nikon) at 340 nm and 380 nm at room temperature. Movies were analyzed with NIS-Elements software (Nikon): background was subtracted, regions of interest for neurons selected, and the 340/380 ratio calculated.

Dark adaptation and light exposure—Male and female adult C57Bl6/J mice (The Jackson Laboratory) were transferred from their normal housing room with a 12: 12 h light:dark cycle into a light-tight dark housing room to maintain constant darkness for 7 days. Animals in the unstimulated (dark) condition were killed and their eyes were enucleated in the dark prior to bringing the body into the light. Animals in the stimulated (light-exposed) condition were removed from the dark room and exposed to normal lighting for either 20 min or 45 min prior to tissue harvesting. Brains were harvested and flash-frozen in an isopentane/dry ice bath. Coronal sections were cut on a cryostat and the slices were mounted on Super Frost Plus slides (Fisher Scientific).

Western Blotting—Neuro2a cells were lysed directly into 2x SDS sample lysis buffer. Samples were sonicated, boiled for 5 min, chilled on ice, then centrifuged at 13,000 RPM

for 3 minutes to remove insoluble material. 10uL of total cell lysate was run on a 8%–12% SDS-PAGE gel and transferred to nitrocellulose. Western blots were blocked in 5% non-fat dry milk in TBST. Primary antibodies included mouse anti-actin (1:20000, MAB1501, EMD Millipore) and mouse anti-FLAG (1:4000, F3165, Sigma). After thorough washing with TBST, blots were incubated with goat anti-mouse 680 (1:5000, cat #20253, Biotium). Fluorescent immunoreactivity was imaged on a LICOR Odyssey.

Electrophysiology—Electrophysiology recordings of hippocampal neurons Whole-cell patch-clamp recordings were performed 5 days post-transfection at room temperature using an EPC10 amplifier and Patchmaster software (HEKA Elektronik, Lambrecht, Germany). Data were sampled at 10 kHz and filtered at 2.9 kHz. Borosilicate glass pipettes (1.5 OD, 0.85 ID; Sutter Instrument Company, Novato, CA) had a resistance of 3–6.5 MΩ when filled with pipette buffer solution (120 mM potassium gluconate, 10 mM KCl, 5 mM MgCl2, 0.6 mM EGTA, 5 mM HEPES, 6 μM CaCl2, 10 mM phosphocreatine disodium, 2 mM Mg-ATP, 0.2 mM GTP, pH = 7.2 adjusted with KOH). Basic external solution contained 126 mM NaCl, 3 mM KCl, 20 mM HEPES, 2 mM CaCl2,1mM MgCl2, 30 mM glucose, and synaptic blockers 20 μM 2-amino-5-phosphonovaleric acid (APV) and 20 mM 6-cyano-7-dinitroquinoxaline-2,3-dione (CNQX), pH = 7.3 adjusted with NaOH. Resting membrane potential was recorded over a 3 s period of zero current injection. Analysis was performed with Igor Pro 6.22A (WaveMetrics, Lake Oswego, OR).

Novel object exploration and hippocampal expression of Fos—dCas9-HDAC8 lentiviruses containing either the Ctrl gRNA targeting LacZ or gRNA1 targeting Fos Enh2 were generated in 293T cells by the Duke University Viral Vector Core Facility and tittered by ELISA (Enh2, 2×10^{10}vg/ml; LacZ, 4×10^{10}vg/ml). Lentiviruses were injected bilaterally into the dorsal hippocampus of adult male C57Bl6/J mice (The Jackson Laboratory) with stereotaxic coordinates AP:−2.3, ML: +/−1.8, DV: −1.8. Two weeks following infection, mice were placed in the open field and allowed to explore three novel objects for a period of 2 hours. Mice were then perfused with 4% paraformaldehyde and brains were coronally sectioned on a freezing microtome for immunostaining with rabbit anti-Cas9 (EnCor RPCA-Cas9-SP, 1:1000) and chicken anti-Fos antibodies (raised against full-length recombinant human c-Fos protein and affinity purified, a gift from J.V. Deng, EnCor, 1:1000). These were detected by anti-rabbit Alexa488 and anti-chicken Cy3, both at 1:500. For Fos protein level in brain slices, these were detected by anti-rabbit Alexa488 and anti-chicken Cy3, both at 1:500. 40X sum projection images were obtained on a Zeiss LSM700 confocal, and either Fos intensity in all cells was quantified in ImageJ or Fos intensity in all Cas9-positive neurons in each image was categorized by an observer blind to condition as background, low, or high.

QUANTIFICATION AND STATISTICAL ANALYSIS

Inference of kinetic parameters from smFISH using BayFish—We modified BayFish (Gómez-Schiavon et al., 2017) to include an explicit delay (τ) in the synthesis of each mature mRNA by replacing time (t) with (t-τ) in the algorithm that integrates the Chemical Master Equation forward in time. This delay arises from transcriptional processing (e.g., elongation, splicing, poly-adenylation, nuclear export). Based on previous work

(Gómez-Schiavon et al., 2017) we only considered a two-state promoter model where the kinetic parameter k_{ON} increased from k^{U}_{ON} (unstimulated) to k^{S}_{ON} (stimulated) upon membrane depolarization. All other inferred parameters (k_{OFF}, μ0, μ1, τ) did not change upon membrane depolarization. For each dataset, we performed the following procedure to calculate the posterior distributions of the model parameters. First, to avoid local maxima (i.e., sub-optimal traps) during the BayFish run, we determined the best starting parameters using a stochastic descent Markov Chain Monte Carto algorithm (Metropolis–Hastings) for 320 randomized initial parameters. The diffusivity (i.e., step size) of each Monte Carlo Step was optimized to assure that most of the chains converge to a local maximum after 10^4 steps. The parameter set with the highest likelihood among the 320 simulations was then set to be the initial condition for the Bayesian analysis (BayFish). We then ran 400 independent BayFish chains for 10^5 Monte Carlo steps. The Bayesian prior was set to be log uniform and the diffusivity (i.e., step size) of BayFish was tuned for each dataset, such that the acceptance rate is near the theoretically-predicted optimum 23.4% (Gelman et al., 1997). After truncating the first 2000 steps from each Monte Carlo chain to allow proper mixing (i.e., discard the burn-in), we checked for convergence by comparing the posterior distribution calculated from the full chain and that calculated from the second half of the chain. The marginal posterior distributions of these two chains were indistinguishable (relative error < 1%). We then concatenated all 400 full chains and computed the marginal posterior distributions from this. The best-fit parameters in Tables S1 and S2 were determined by finding those parameters in the concatenated chain that had the highest likelihood of generating the observed data. When comparing the marginal posteriors between two datasets in Figure S6, we calculated the coefficient of overlap (Inman and Bradley, 1989) by discretizing the real-valued samples into 5000 bins in the projected parameter space.

Statistical Analyses—Unless otherwise indicated, all data presented are the average of at least two biological replicates from each of at least two independent experiments. Statistical analysis was matched to the data structure. All distributions of smFISH data were analyzed by the Kolmogorov–Smirnov test, which is a non-parametric test that tests against the null hypothesis that two datasets arise from the same distribution. Unless otherwise indicated, remaining data were analyzed by ANOVA or Student's unpaired t test depending on the number of samples being compared (2 or more than 2). In all cases a $p < 0.05$ was considered significant. Bar and line graphs show mean values and all error bars show SEM. Statistical values for all experiments are presented in the figure legends.

Supplementary Material

Refer to Web version on PubMed Central for supplementary material.

ACKNOWLEDGMENTS

This work was supported by NIH grant R21/R33 DA041878 (to A.E.W. and C.A.G.), NIH New Innovator Award DP2 OD008654-01 (N.E.B.), Burroughs Wellcome Fund CASI Award BWF 1005769.01 (N.E.B.), Allen Distinguished Investigator Award from the Paul G. Allen Frontiers Group (C.A.G. and A.E.W.), R01DA036865 (C.A.G.), and the Center for Nonlinear Studies, Los Alamos National Laboratory (Y.T.L.). We thank Isaac Hilton (Duke University) for sharing CRISPR plasmids, Jie V. Deng for help with the stereotaxic injections and the gift of the Fos antibody, Josh Black and Tyler Klann for construction of the viral vectors, Boris Kantor and the Duke Viral

Vector Core Facility for lentiviral production, Daniel Larson (National Cancer Institute) for technical support with the smFISH methods, and Sridhar Raghavachari (Duke University) for inspiration.

REFERENCES

Bhatt DM, Pandya-Jones A, Tong AJ, Barozzi I, Lissner MM, Natoli G, Black DL, and Smale ST (2012). Transcript dynamics of proinflammatory genes revealed by sequence analysis of subcellular RNA fractions. Cell 150, 279–290. [PubMed: 22817891]

Bito H, Deisseroth K, and Tsien RW (1996). CREB phosphorylation and dephosphorylation: a Ca(2+)- and stimulus duration-dependent switch for hippocampal gene expression. Cell 87, 1203–1214. [PubMed: 8980227]

Blow MJ, McCulley DJ, Li Z, Zhang T, Akiyama JA, Holt A, Plajzer-Frick I, Shoukry M, Wright C, Chen F, et al. (2010). ChIP-seq identification of weakly conserved heart enhancers. Nat. Genet. 42, 806–810. [PubMed: 20729851]

Chen L-F, Zhou AS, and West AE (2017). Transcribing the connectome: roles for transcription factors and chromatin regulators in activity-dependent synapse development. J. Neurophysiol. 118, 755–770. [PubMed: 28490640]

Dar RD, Razooky BS, Singh A, Trimeloni TV, McCollum JM, Cox CD, Simpson ML, and Weinberger LS (2012). Transcriptional burst frequency and burst size are equally modulated across the human genome. Proc. Natl. Acad. Sci. USA 109, 17454–17459. [PubMed: 23064634]

Das S, Moon HC, Singer RH, and Park HY (2018). A transgenic mouse for imaging activity-dependent dynamics of endogenous Arc mRNA in live neurons. Sci. Adv. 4, eaar3448. [PubMed: 29938222]

Dolmetsch RE, Pajvani U, Fife K, Spotts JM, and Greenberg ME (2001). Signaling to the nucleus by an L-type calcium channel-calmodulin complex through the MAP kinase pathway. Science 294, 333–339. [PubMed: 11598293]

Dorighi KM, Swigut T, Henriques T, Bhanu NV, Scruggs BS, Nady N, Still CD, Garcia BA, 2nd, Adelman K, and Wysocka J (2017). Mll3 and Mll4 facilitate enhancer RNA synthesis and transcription from promoters independently of H3K4 monomethylation. Mol. Cell 66, 568–576. [PubMed: 28483418]

Fukaya T, Lim B, and Levine M (2016). Enhancer control of transcriptional bursting. Cell 166, 358–368. [PubMed: 27293191]

Gelman A, Gilks WR, and Roberts GO (1997). Weak convergence and optimal scaling of random walk Metropolis algorithms. Ann. Appl. Probab. 7, 110–120.

Ghiretti AE, Moore AR, Brenner RG, Chen L-F, West AE, Lau NC, Van Hooser SD, and Paradis S (2014). Rem2 is an activity-dependent negative regulator of dendritic complexity *in vivo*. J. Neurosci. 34, 392–407. [PubMed: 24403140]

Gómez-Schiavon M, Chen L-F, West AE, and Buchler NE (2017). BayFish: Bayesian inference of transcription dynamics from population snapshots of single-molecule RNA FISH in single cells. Genome Biol. 18, 164. [PubMed: 28870226]

Gräff J, and Tsai L-H (2013). Histone acetylation: molecular mnemonics on the chromatin. Nat. Rev. Neurosci. 14, 97–111. [PubMed: 23324667]

Greer PL, and Greenberg ME (2008). From synapse to nucleus: calcium-dependent gene transcription in the control of synapse development and function. Neuron 59, 846–860. [PubMed: 18817726]

Halder R, Hennion M, Vidal RO, Shomroni O, Rahman R-U, Rajput A, Centeno TP, van Bebber F, Capece V, Garcia Vizcaino JC, et al. (2016). DNA methylation changes in plasticity genes accompany the formation and maintenance of memory. Nat. Neurosci. 19, 102–110. [PubMed: 26656643]

Heintzman ND, Hon GC, Hawkins RD, Kheradpour P, Stark A, Harp LF, Ye Z, Lee LK, Stuart RK, Ching CW, et al. (2009). Histone modifications at human enhancers reflect global cell-type-specific gene expression. Nature 459, 108–112. [PubMed: 19295514]

Heller EA, Cates HM, Peña CJ, Sun H, Shao N, Feng J, Golden SA, Herman JP, Walsh JJ, Mazei-Robison M, et al. (2014). Locus-specific epigenetic remodeling controls addiction- and depression-related behaviors. Nat. Neurosci. 17, 1720–1727. [PubMed: 25347353]

Hilton IB, D'Ippolito AM, Vockley CM, Thakore PI, Crawford GE, Reddy TE, and Gersbach CA (2015). Epigenome editing by a CRISPR-Cas9-based acetyltransferase activates genes from promoters and enhancers. Nat. Biotechnol. 33, 510–517. [PubMed: 25849900]

Hrvatin S, Hochbaum DR, Nagy MA, Cicconet M, Robertson K, Cheadle L, Zilionis R, Ratner A, Borges-Monroy R, Klein AM, et al. (2018). Single-cell analysis of experience-dependent transcriptomic states in the mouse visual cortex. Nat. Neurosci. 21, 120–129. [PubMed: 29230054]

Inman HF, and Bradley EL, Jr. (1989). The overlapping coefficient as a measure of agreement between probability distributions and point estimation of the overlap of two normal densities. Commun. Stat. Theory Methods 18, 3851–3874.

Jaeger BN, Linker SB, Parylak SL, Barron JJ, Gallina IS, Saavedra CD, Fitzpatrick C, Lim CK, Schafer ST, Lacar B, et al. (2018). A novel environment-evoked transcriptional signature predicts reactivity in single dentate granule neurons. Nat. Commun. 9, 3084. [PubMed: 30082781]

Jones JC, Phatnani HP, Haystead TA, MacDonald JA, Alam SM, and Greenleaf AL (2004). C-terminal repeat domain kinase I phosphorylates Ser2 and Ser5 of RNA polymerase II C-terminal domain repeats. J. Biol. Chem. 279, 24957–24964. [PubMed: 15047695]

Jonkers I, and Lis JT (2015). Getting up to speed with transcription elongation by RNA polymerase II. Nat. Rev. Mol. Cell Biol. 16, 167–177. [PubMed: 25693130]

Joo JY, Schaukowitch K, Farbiak L, Kilaru G, and Kim TK (2016). Stimulus-specific combinatorial functionality of neuronal c-fos enhancers. Nat. Neurosci. 19, 75–83. [PubMed: 26595656]

Kim TK, Hemberg M, Gray JM, Costa AM, Bear DM, Wu J, Harmin DA, Laptewicz M, Barbara-Haley K, Kuersten S, et al. (2010). Wide-spread transcription at neuronal activity-regulated enhancers. Nature 465, 182–187. [PubMed: 20393465]

Korb E, Herre M, Zucker-Scharff I, Darnell RB, and Allis CD (2015). BET protein Brd4 activates transcription in neurons and BET inhibitor Jq1 blocks memory in mice. Nat. Neurosci. 18, 1464–1473. [PubMed: 26301327]

Larson DR, Zenklusen D, Wu B, Chao JA, and Singer RH (2011). Real-time observation of transcription initiation and elongation on an endogenous yeast gene. Science 332, 475–478. [PubMed: 21512033]

Larson DR, Fritzsch C, Sun L, Meng X, Lawrence DS, and Singer RH (2013). Direct observation of frequency modulated transcription in single cells using light activation. eLife 2, e00750. [PubMed: 24069527]

Lee PR, Cohen JE, Iacobas DA, Iacobas S, and Fields RD (2017). Gene networks activated by specific patterns of action potentials in dorsal root ganglia neurons. Sci. Rep. 7, 43765. [PubMed: 28256583]

Leslie JH, and Nedivi E (2011). Activity-regulated genes as mediators of neural circuit plasticity. Prog. Neurobiol. 94, 223–237. [PubMed: 21601615]

Levine M, Cattoglio C, and Tjian R (2014). Looping back to leap forward: transcription enters a new era. Cell 157, 13–25. [PubMed: 24679523]

Liu XS, Wu H, Ji X, Stelzer Y, Wu X, Czauderna S, Shu J, Dadon D, Young RA, and Jaenisch R (2016). Editing DNA methylation in the mammalian genome. Cell 167, 233–247. [PubMed: 27662091]

Lyons MR, and West AE (2011). Mechanisms of specificity in neuronal activity-regulated gene transcription. Prog. Neurobiol. 94, 259–295. [PubMed: 21620929]

Lyons MR, Chen LF, Deng JV, Finn C, Pfenning AR, Sabhlok A, Wilson KM, and West AE (2016). The transcription factor calcium-response factor limits NMDA receptor-dependent transcription in the developing brain. J. Neurochem. 137, 164–176. [PubMed: 26826701]

Malik AN, Vierbuchen T, Hemberg M, Rubin AA, Ling E, Couch CH, Stroud H, Spiegel I, Farh KK, Harmin DA, and Greenberg ME (2014). Genome-wide identification and characterization of functional neuronal activity-dependent enhancers. Nat. Neurosci. 17, 1330–1339. [PubMed: 25195102]

Molina N, Suter DM, Cannavo R, Zoller B, Gotic I, and Naef F (2013). Stimulus-induced modulation of transcriptional bursting in a single mammalian gene. Proc. Natl. Acad. Sci. USA 110, 20563–20568. [PubMed: 24297917]

Mueller F, Senecal A, Tantale K, Marie-Nelly H, Ly N, Collin O, Basyuk E, Bertrand E, Darzacq X, and Zimmer C (2013). FISH-quant: automatic counting of transcripts in 3D FISH images. Nat. Methods 10, 277–278. [PubMed: 23538861]

Nicolas D, Zoller B, Suter DM, and Naef F (2018). Modulation of transcriptional burst frequency by histone acetylation. Proc. Natl. Acad. Sci. USA 115, 7153–7158. [PubMed: 29915087]

Nord AS, Blow MJ, Attanasio C, Akiyama JA, Holt A, Hosseini R, Phouanenavong S, Plajzer-Frick I, Shoukry M, Afzal V, et al. (2013). Rapid and pervasive changes in genome-wide enhancer usage during mammalian development. Cell 155, 1521–1531. [PubMed: 24360275]

Raj A, van den Bogaard P, Rifkin SA, van Oudenaarden A, and Tyagi S (2008). Imaging individual mRNA molecules using multiple singly labeled probes. Nat. Methods 5, 877–879. [PubMed: 18806792]

Saha RN, Wissink EM, Bailey ER, Zhao M, Fargo DC, Hwang J-Y, Daigle KR, Fenn JD, Adelman K, and Dudek SM (2011). Rapid activity-induced transcription of Arc and other IEGs relies on poised RNA polymerase II. Nat. Neurosci. 14, 848–856. [PubMed: 21623364]

Schindelin J, Arganda-Carreras I, Frise E, Kaynig V, Longair M, Pietzsch T, Preibisch S, Rueden C, Saalfeld S, Schmid B, et al. (2012). Fiji: an open-source platform for biological-image analysis. Nat. Methods 9, 676–682. [PubMed: 22743772]

Senecal A, Munsky B, Proux F, Ly N, Braye FE, Zimmer C, Mueller F, and Darzacq X (2014). Transcription factors modulate c-Fos transcriptional bursts. Cell Rep. 8, 75–83. [PubMed: 24981864]

Shao W, and Zeitlinger J (2017). Paused RNA polymerase II inhibits new transcriptional initiation. Nat. Genet. 49, 1045–1051. [PubMed: 28504701]

Shyu AB, Greenberg ME, and Belasco JG (1989). The c-fos transcript is targeted for rapid decay by two distinct mRNA degradation pathways. Genes Dev. 3, 60–72. [PubMed: 2496006]

Su Y, Shin J, Zhong C, Wang S, Roychowdhury P, Lim J, Kim D, Ming GL, and Song H (2017). Neuronal activity modifies the chromatin accessibility landscape in the adult brain. Nat. Neurosci 20, 476–483. [PubMed: 28166220]

Suter DM, Molina N, Gatfield D, Schneider K, Schibler U, and Naef F (2011). Mammalian genes are transcribed with widely different bursting kinetics. Science 332, 472–474. [PubMed: 21415320]

Symmons O, and Raj A (2016). What's luck got to do with it: single cells, multiple fates, and biological nondeterminism. Mol. Cell 62, 788–802. [PubMed: 27259209]

Thakore PI, Black JB, Hilton IB, and Gersbach CA (2016). Editing the epigenome: technologies for programmable transcription and epigenetic modulation. Nat. Methods 13, 127–137. [PubMed: 26820547]

Tyssowski KM, DeStefino NR, Cho J-H, Dunn CJ, Poston RG, Carty CE, Jones RD, Chang SM, Romeo P, Wurzelmann MK, et al. (2018). Different neuronal activity patterns induce different gene expression programs. Neuron 98, 530–546. [PubMed: 29681534]

VanElzakker M, Fevurly RD, Breindel T, and Spencer RL (2008). Environmental novelty is associated with a selective increase in Fos expression in the output elements of the hippocampal formation and the perirhinal cortex. Learn. Mem. 15, 899–908. [PubMed: 19050162]

Vasanwala FH, Kusam S, Toney LM, and Dent AL (2002). Repression of AP-1 function: a mechanism for the regulation of Blimp-1 expression and B lymphocyte differentiation by the B cell lymphoma-6 protooncogene. J. Immunol 169, 1922–1929. [PubMed: 12165517]

Vera M, Biswas J, Senecal A, Singer RH, and Park HY (2016). Single-cell and single-molecule analysis of gene expression regulation. Annu. Rev. Genet. 50, 267–291. [PubMed: 27893965]

Visel A, Taher L, Girgis H, May D, Golonzhka O, Hoch RV, McKinsey GL, Pattabiraman K, Silberberg SN, Blow MJ, et al. (2013). A high-resolution enhancer atlas of the developing telencephalon. Cell 152, 895–908. [PubMed: 23375746]

Whitaker LR, Warren BL, Venniro M, Harte TC, McPherson KB, Beidel J, Bossert JM, Shaham Y, Bonci A, and Hope BT (2017). Bidirectional modulation of intrinsic excitability in rat prelimbic cortex neuronal ensembles and non-ensembles after operant learning. J. Neurosci. 37, 8845–8856. [PubMed: 28779019]

Winter GE, Mayer A, Buckley DL, Erb MA, Roderick JE, Vittori S, Reyes JM, di Iulio J, Souza A, Ott CJ, et al. (2017). BET bromodomain proteins function as master transcription elongation factors independent of CDK9 recruitment. Mol. Cell 67, 5–18. [PubMed: 28673542]

Wu S, Li K, Li Y, Zhao T, Li T, Yang Y-F, and Qian W (2017). Independent regulation of gene expression level and noise by histone modifications. PLoS Comput. Biol. 13, e1005585. [PubMed: 28665997]

Xu J, Bartolome CL, Low CS, Yi X, Chien C-H, Wang P, and Kong D (2018). Genetic identification of leptin neural circuits in energy and glucose homeostases. Nature 556, 505–509. [PubMed: 29670283]

Zhai S, Ark ED, Parra-Bueno P, and Yasuda R (2013). Long-distance integration of nuclear ERK signaling triggered by activation of a few dendritic spines. Science 342, 1107–1111. [PubMed: 24288335]

Zheng Y, Shen W, Zhang J, Yang B, Liu Y-N, Qi H, Yu X, Lu S-Y, Chen Y, Xu Y-Z, et al. (2018). CRISPR interference-based specific and efficient gene inactivation in the brain. Nat. Neurosci. 21, 447–454. [PubMed: 29403034]

Zhou H, Liu J, Zhou C, Gao N, Rao Z, Li H, Hu X, Li C, Yao X, Shen X, et al. (2018). *In vivo* simultaneous transcriptional activation of multiple genes in the brain using CRISPR-dCas9-activator transgenic mice. Nat. Neurosci. 21, 440–446. [PubMed: 29335603]

Zippo A, Serafini R, Rocchigiani M, Pennacchini S, Krepelova A, and Oliviero S (2009). Histone crosstalk between H3S10ph and H4K16ac generates a histone code that mediates transcription elongation. Cell 138, 1122–1136. [PubMed: 19766566]

Highlights

- We quantify transcriptional bursting dynamics of *Fos* and *Npas4* in neurons
- Bidirectional regulation of enhancer acetylation tunes *Fos* transcriptional bursts
- Fos driven by enhancer epigenome editing alters neuronal physiology
- Enhancer-recruited dCas9-HDAC8 impairs Fos induction in neurons *in vivo*

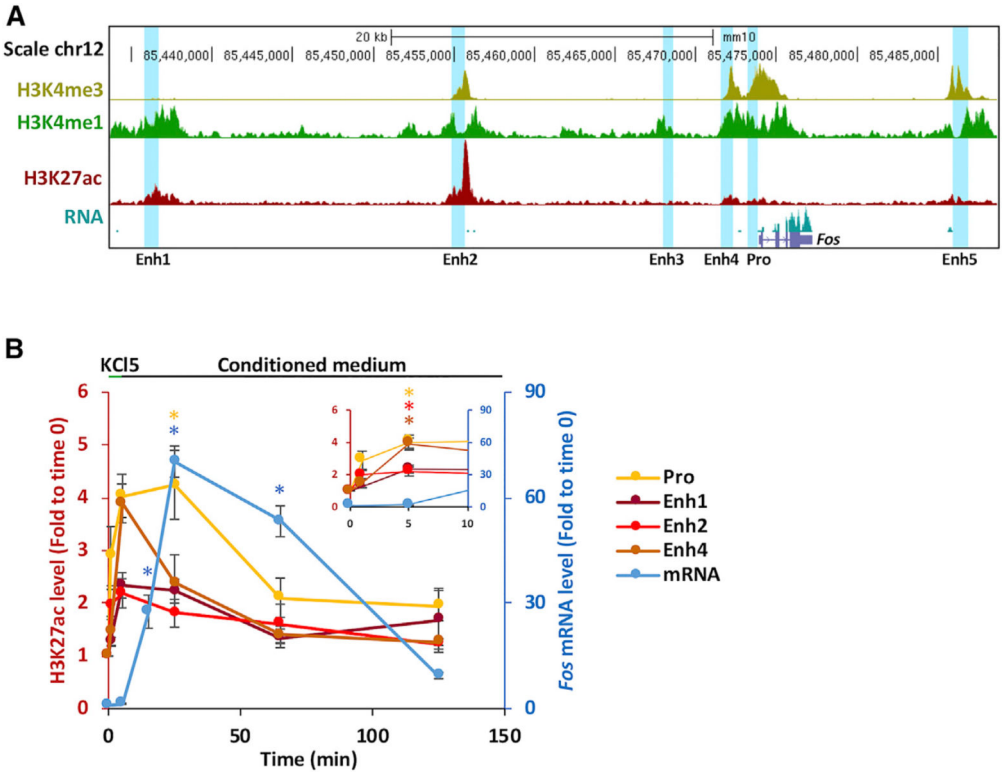

Figure 1. Membrane Depolarization Transiently Induces H3K27ac at *Fos* Regulatory Elements

(A) Chromatin landscape of *Fos* in embryonic day (E) 16.5 mouse forebrain. Blue vertical bars show putative *Fos* enhancers and the promoter (GEO: GSE82453, GSE82464, GSE82690, and GSE78323).

(B) H3K27ac ChIP-qPCR at the *Fos* promoter (yellow) and three distal enhancers (dark red, Enh1; red, Enh2; and brown, Enh4) following 5 min membrane depolarization of primary mouse cortical neurons. Time course of *Fos* mRNA is shown in blue. Following the 5 min stimulation (green bar above graph, KCl5), the high KCl solution is removed and cells are returned to conditioned medium (black bar above graph). Cell conditions are noted throughout the manuscript as basal (immediately before membrane depolarization), KCl5 (immediately following membrane depolarization), or KCl5+X (X min following return to conditioned medium). The inset shows an enlargement of the first 10 min.

n for ChIP-qPCR: 0 min = 6, 1 min = 4, 5 min = 6, 25 min = 6, 65 min = 5, 125 min = 5. n for mRNA = 4/time point. Data are represented as mean ± SEM. One-way ANOVA with Bonferroni post hoc tests, mRNA: $F(5,18) = 81.18$, $p < 0.01$; H3K27ac: promoter (Pro) $F(5,26) = 5.98$, $p < 0.01$, Enh1 $F(5,26) = 2.54$, $p = 0.05$, Enh2 $F(5,26) = 3.48$, $p = 0.02$, Enh4 $F(5,26) = 5.90$, $p < 0.01$; H3K27ac at 5 min: Pro $p = 0.04$, Enh2 $p = 0.02$, Enh4 $p < 0.01$; mRNA at 15 min: $p < 0.01$ compared with time 0. *$p < 0.05$ compared with time 0.

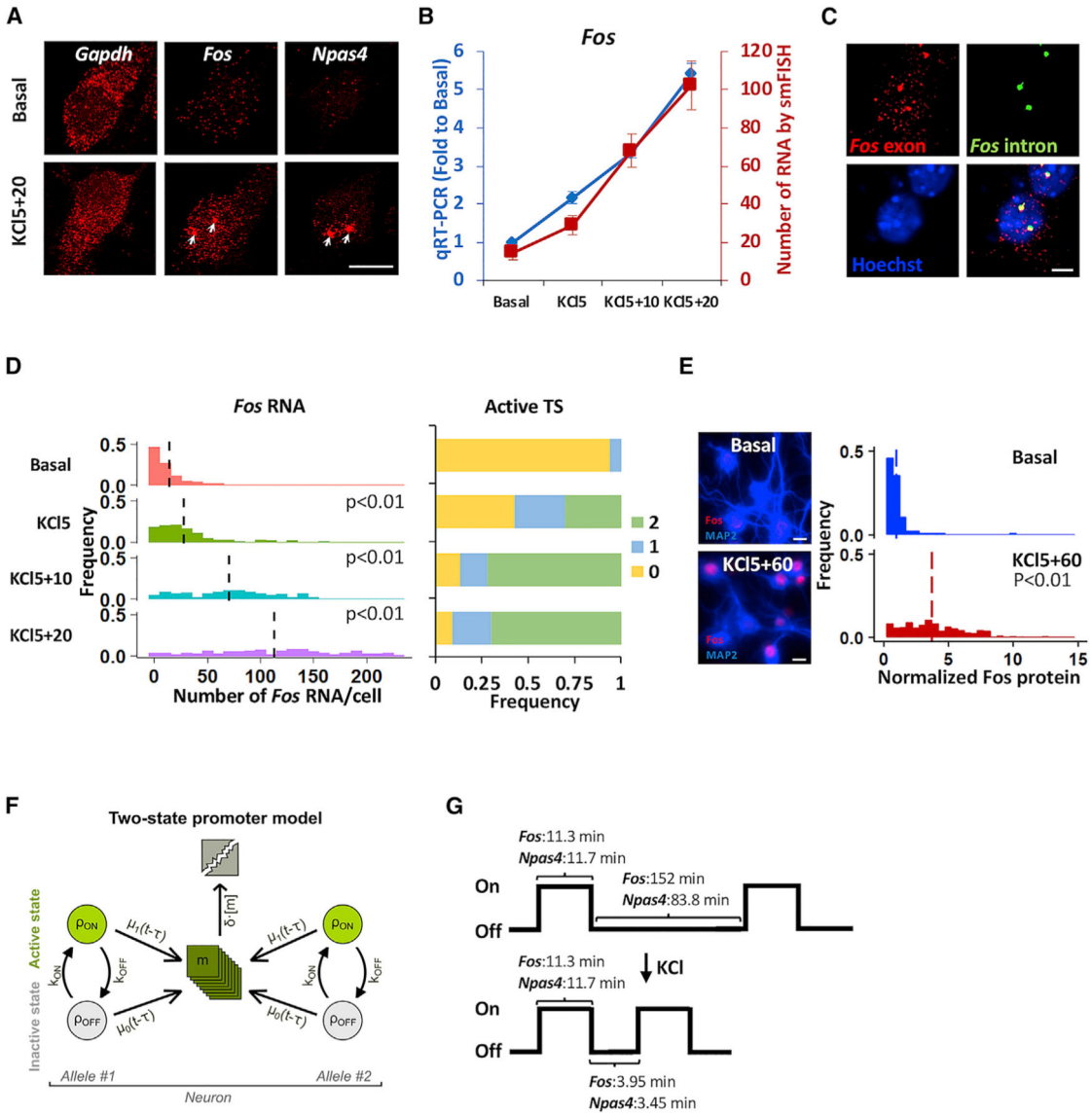

Figure 2. Transcriptional Bursting of *Fos* in Neurons

(A) Representative smFISH images for the indicated mRNAs in primary mouse hippocampal neurons before and 20 min after a 5 min exposure to 55 mM KCl. White arrows show the two alleles in the nucleus. Scale bar, 5 μm. *Gapdh* is shown as a non-membrane depolarization-inducible control.

(B) Average *Fos* RNA levels at different time points before (basal) and after a 5 min pulse of KCl by smFISH (red line) and qRT-PCR (blue line). Error bars are 95% confidence interval (CI) for smFISH and SEM for qRT-PCR. n = 3 biological replicates/condition.

(C) Representative dual-color smFISH images for *Fos* exon and *Fos* intron in single neurons at 20 min following a 5 min exposure to 55 mM KCl. Scale bar, 5 μm.

(D) Observed distributions of *Fos* RNA and active transcription sites (TSs) per single cell by smFISH. Dashed lines show average RNA number for each group. Data were analyzed by a Kolmogorov-Smirnov (K-S) test. $p < 0.01$ basal versus KCl5, $p < 0.01$ basal versus

KCl5+10, $p < 0.01$ basal versus KCl5+20. Basal, n = 173; KCl5, n = 174; KCl5+10, n = 122; KCl5+20, n = 115 neurons from 3 biological replicates.

(E) Fos protein levels in single primary mouse hippocampal neurons, before (basal, blue) and 60 min after (KCl5+60, red) a 5 min exposure to 55 mM KCl. Dashed lines show average for each group. Data were analyzed by K-S test. $p < 0.01$ basal versus KCl5+60. Basal, n = 172; KCl5+60, n = 345 neurons from 2 biological replicates. Scale bar, 5 μm.

(F) Schematic diagram of the two-state promoter model. The promoter of each allele can be in either an active (ρ_{ON}) or an inactive (ρ_{OFF}) state. Each allele synthesizes mature mRNA molecules (m) with the rate μ_1 or μ_0 if the promoter is active or inactive, respectively, and the synthesis of each mature mRNA is delayed by a processing time τ. Stochastic transitions between promoter states occur with a promoter activation rate k_{ON} and a promoter deactivation rate k_{OFF}. Finally, each mRNA is degraded with rate δ.

(G) Cartoon summarizing the best-fit model parameters in Table S1 for the mean duration of time that *Fos* and *Npas4* promoters are active or inactive. Membrane depolarization predominantly increases k_{ON}, thus decreasing the mean “off” duration of a promoter and increasing burst frequency.

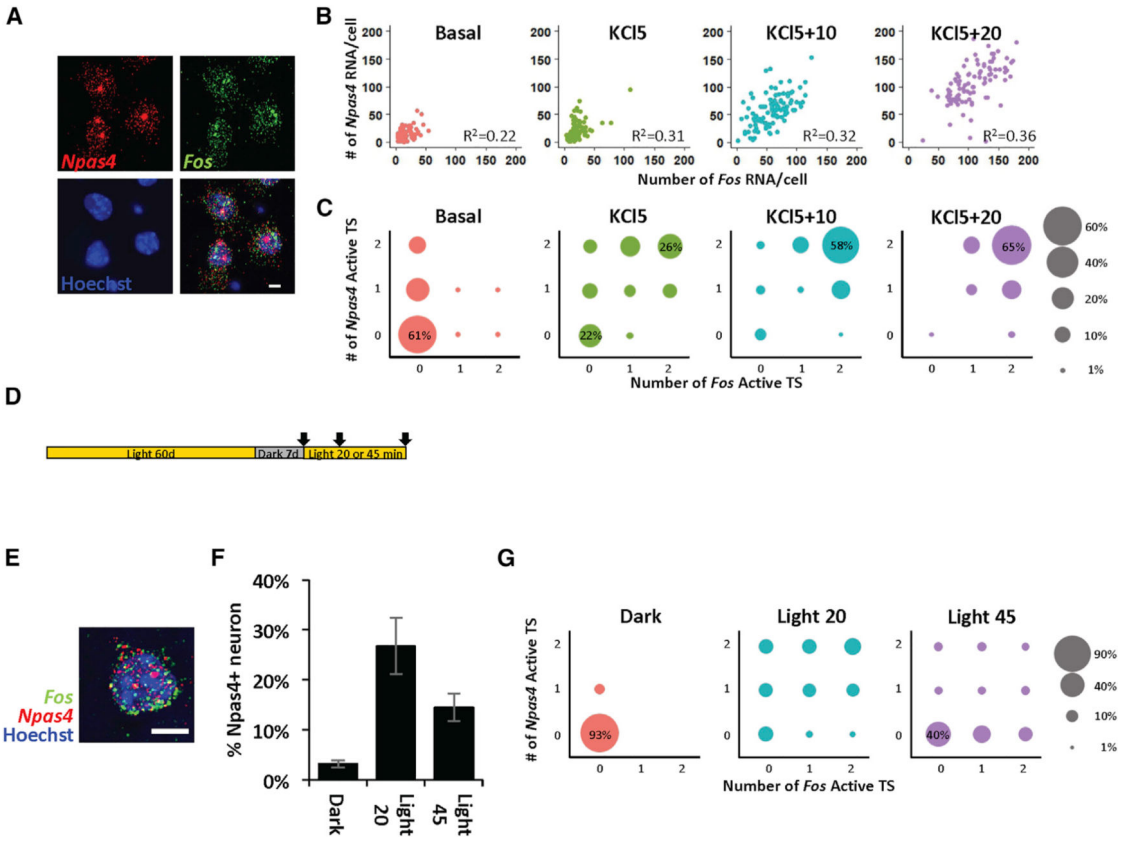

Figure 3. Allele-Intrinsic Variability of *Fos* and *Npas4* Bursting in Neurons in Culture and *In Vivo*

(A) Representative dual-color smFISH images for *Fos* and *Npas4* in single neurons at 20 min following a 5 min exposure to 55 mM KCl. Scale bar, 5 μm.

(B and C) Scatterplot of (B) RNA and distribution of (C) active TS in single neurons at different time points by dual-color smFISH. Basal, n = 93; KCl5, n = 100; KCl5+10, n = 104; KCl5+20, n = 99 neurons from 2 biological replicates.

(D) Experimental timeline of light exposure experiment.

(E) Representative dual-color smFISH images for *Fos* and *Npas4* in single neurons in the visual cortex from mouse exposed to 20 min light. Scale bar, 5 μm.

(F) Percentage of Npas4-positive neurons in the visual cortex. Light 20 min, p = 0.05; light 45 min, p = 0.05 compared with dark. n = 2 mice/condition.

(G) Number of active *Fos* and *Npas4* TS in *Npas4*-positive neurons at different time points by dual-color smFISH. Dark, n = 1,531; light 20 min, n = 1,731; light 45 min, n = 2,106 neurons. n = 2 mice/condition.

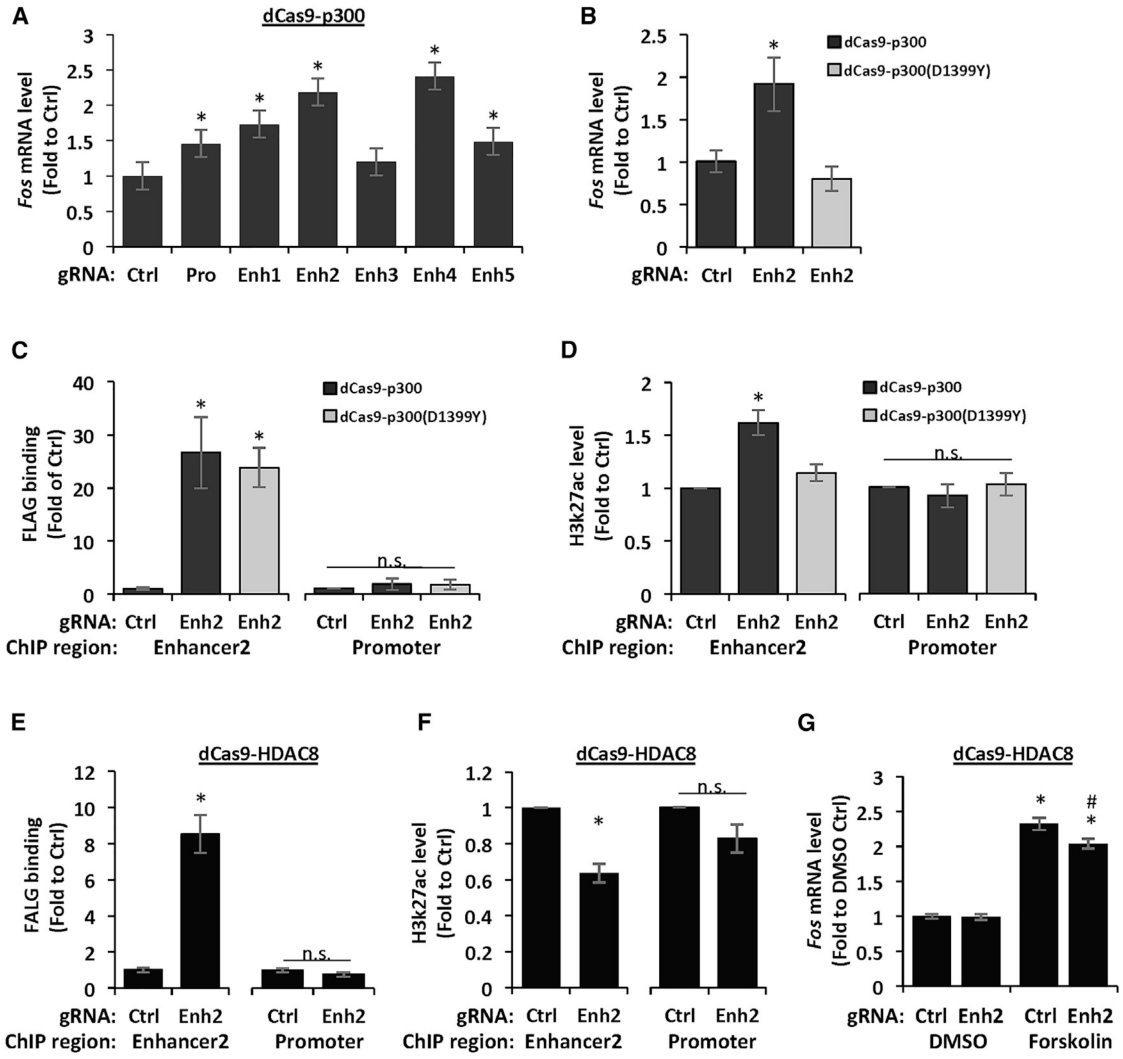

Figure 4. dCas9-p300 and dCas9-HDAC8 Bidirectionally Regulate H3K27ac at Enhancers and *Fos* Expression in N2A Cells

(A) Level of *Fos* mRNA in N2A cells cotransfected with dCas-p300 and gRNAs targeting the *Fos* promoter or the indicated putative distal *Fos* enhancers. Control (Ctrl): n = 6; Pro: p = 0.01, n = 4; Enh1: p < 0.01, n = 3; Enh2: p < 0.01, n = 7; Enh3: p = 0.07, n = 7; Enh4: p < 0.01, n = 6; Enh5: p < 0.01, n = 7 compared with Ctrl. *p < 0.05 compared with Ctrl.

(B) Fos mRNA levels in N2A cells cotransfected with dCas-p300 or an acetyltransferase dead (D1933Y) version of dCas-p300, along with either a Ctrl gRNA plasmid or a pool of gRNAs targeted to *Fos* Enh2. p = 0.04 Ctrl versus dCas9-p300 at Enh2, p = 0.32 Ctrl versus dCas9-p300DY at Enh2. n = 4/condition. *p < 0.05 compared with Ctrl.

(C) FLAG binding level at *Fos* promoter and Enh2 in N2A cells cotransfected with either a Ctrl gRNA plasmid or a pool of gRNAs targeted to *Fos* Enh2 and the indicated FLAG fusion dCas9 variants. Enhancer 2: p = 0.02 Ctrl versus dCas9-p300 at Enh2, p < 0.01 Ctrl versus dCas9-p300DY at Enh2; promoter: p = 0.51 Ctrl versus dCas9-p300 at Enh2, p = 0.47 Ctrl versus dCas9-p300DY at Enh2. n = 3/condition. *p < 0.05 compared with Ctrl.

(D) H3K27ac ChIP-qPCR enrichment at *Fos* promoter and Enh2 in N2A cells cotransfected with either a Ctrl gRNA plasmid or a pool of gRNAs targeted to *Fos* Enh2 and the indicated dCas-p300 proteins. Enhancer 2: $p < 0.01$ Ctrl versus dCas9-p300 at Enh2, $p = 0.11$ Ctrl versus dCas9-p300DY at Enh2; promoter: $p = 0.48$ Ctrl versus dCas9-p300 at Enh2, $p = 0.78$ Ctrl versus dCas9-p300DY at Enh2. n = 5/condition. *$p < 0.05$ compared with Ctrl.
(E) FLAG binding level at *Fos* promoter and Enh2 in N2A cells cotransfected with either a Ctrl gRNA plasmid or a pool of gRNAs targeted to *Fos* Enh2 and the indicated FLAG fusion dCas9-HDAC8. Enhancer 2, $p < 0.01$ Ctrl versus dCas9-HDAC8 at Enh2; promoter, $p = 0.2$ Ctrl versus dCas9-HDAC8 at Enh2. n = 6/condition. *$p < 0.05$.
(F) H3K27ac ChIP-qPCR enrichment at *Fos* promoter and enhancer 2 in N2A cells cotransfected with either a Ctrl gRNA plasmid or a pool of gRNAs targeted to *Fos* Enh2 and the indicated dCas-Hdac8 proteins. Enhancer 2, $p < 0.01$ Ctrl versus dCas9-HDAC8 at Enh2; promoter, $p = 0.05$ Ctrl versus dCas9-HDAC8 at Enh2. n = 5/condition. *$p < 0.05$ compared with Ctrl.
(G) Fos mRNA levels in N2A cells cotransfected with dCas-HDAC8, along with either a Ctrl gRNA plasmid or a pool of gRNAs targeted to *Fos* Enh2, and treated with the indicated drugs. $p < 0.01$ Ctrl, Forskolin versus DMSO; $p < 0.01$ Enh2, Forskolin versus DMSO; $p = 0.86$ DMSO, Enh2 versus Ctrl; $p = 0.02$ Forskolin, Enh2 versus Ctrl. n = 8/condition. *$p < 0.05$ compared with DMSO, #$p < 0.05$ compared with Ctrl plus forskolin.

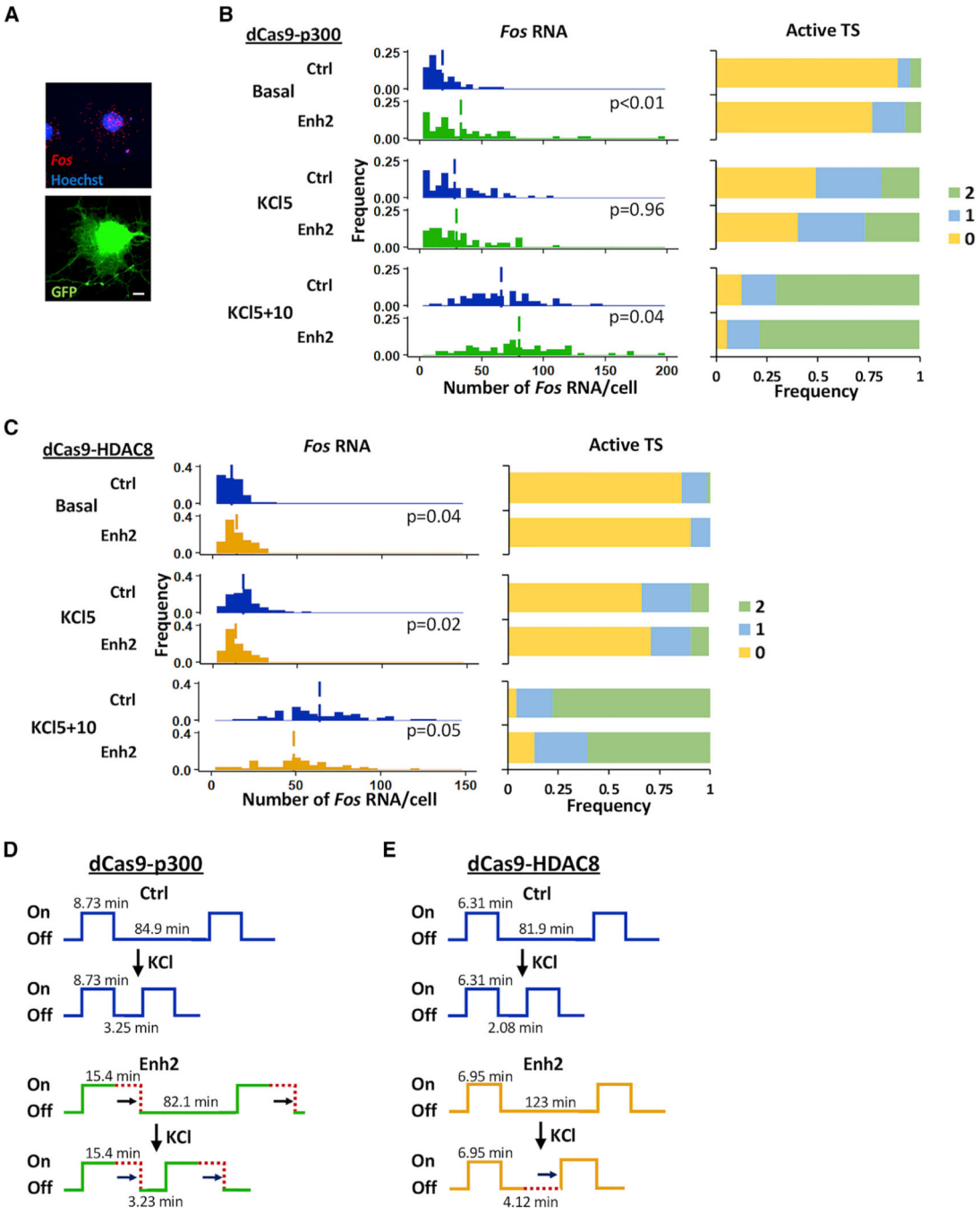

Figure 5. Bidirectional Regulation of *Fos* Transcription by Recruitment of dCas9-p300 or dCas9-HDAC8 to *Fos* Enhancer 2 in Neurons

(A) Representative smFISH image of hippocampal neurons transfected with dCas-p300 and gRNAs at 10 min after a 5 min exposure to 55 mM KCl. GFP expressed from gRNA plasmids.

(B) Observed distributions of *Fos* RNA and active TS measured by smFISH in single neurons at different time points before (basal), after a 5 min pulse of KCl (KCl5), and 10 min after the pulse (KCl5+10). Cultured mouse hippocampal neurons were cotransfected with dCas-p300 and indicated gRNAs. Dashed lines show the average RNA number for each

group. Data were analyzed by K-S test. $p < 0.01$ basal, $p = 0.96$ KCl5, $p = 0.04$ KCl5+10 compared with Ctrl. Basal: Ctrl n = 62, Enh2 n = 63; KCl5: Ctrl n = 60, Enh2 n = 63; KCl5+10: Ctrl n = 60, Enh2 n = 78 neurons per group from 3 biological replicates.
(C) Observed distributions of *Fos* RNA and active TS measured by smFISH in single neurons at time points before (basal), after a 5 min pulse of KCl (KCl5), and 10 min after the pulse (KCl5+10). Cultured mouse hippocampal neurons were cotransfected with dCas-HDAC8 and indicated gRNAs. Dashed lines show average RNA number for each group. Data were analyzed by K-S test. $p = 0.04$ basal, $p = 0.02$ KCl5, $p = 0.05$ KCl5+10 compared with Ctrl. Basal: Ctrl n = 65, Enh2 n = 64; KCl5: Ctrl n = 71, Enh2 n = 64; KCl5+10: Ctrl n = 68, Enh2 n = 61 neurons per group from 3 biological replicates.
(D and E) Cartoon summarizing the best-fit model parameters in Table S2 for the mean duration of time that *Fos* is active or inactive for (D) dCas9-p300 and (E) dCas9-HDAC8 recruitment to *Fos* Enh2.

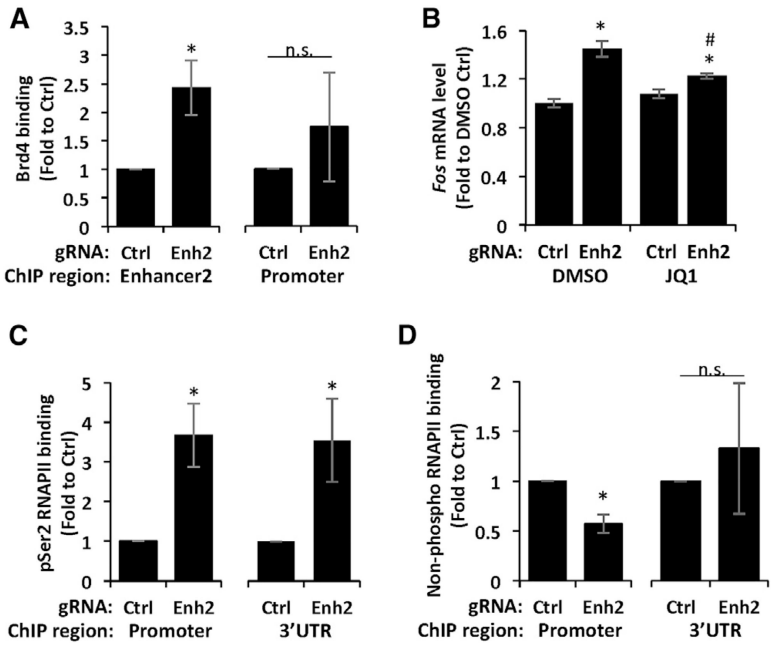

Figure 6. Enhancer H3K27ac Promotes *Fos* Transcriptional Elongation by Recruiting Brd4

(A) Brd4 ChIP-qPCR enrichment at *Fos* promoter and Enh2 in N2A cells cotransfected with dCas-p300, along with either a Ctrl gRNA plasmid or a pool of gRNAs targeted to *Fos* Enh2. Enhancer 2, $p = 0.02$; promoter, $p = 0.46$ compared with Ctrl. n = 5/condition.

(B) *Fos* mRNA levels in N2A cells cotransfected with dCas-p300, along with either a Ctrl gRNA plasmid or a pool of gRNAs targeted to *Fos* Enh2, and treated with the indicated drugs. DMSO, $p < 0.01$ Ctrl versus Enh2; JQ1, $p < 0.01$ Ctrl versus Enh2; Ctrl, $p = 0.12$ DMSO versus JQ1; Enh2, $p < 0.01$ DMSO versus JQ1. *$p < 0.05$ Ctrl versus Enh2, #$p < 0.05$ DMSO versus JQ1 for Enh2. n = 5/condition.

(C) Pol II phosphorylated at Ser2 (pSer2) ChIP-qPCR enrichment at *Fos* promoter and 3' UTR in N2A cells cotransfected with dCas-p300, along with either a Ctrl gRNA plasmid or a pool of gRNAs targeted to *Fos* Enh2. Pro, $p = 0.01$ Enh2; 3' UTR, $p = 0.04$ compared with Ctrl. n = 6/condition. Data are represented as mean ± SEM; two-tailed Student's t test, *$p < 0.05$ compared with Ctrl. n.s., not significant.

(D) Non-phosphorylated Pol II ChIP-qPCR enrichment at *Fos* promoter and 3' UTR in N2A cells cotransfected with dCas-p300, along with either a Ctrl gRNA plasmid or a pool of gRNAs targeted to Fos Enh2. Pro, $p < 0.01$ Enh2; 3' UTR, $p = 0.63$ compared with Ctrl. n = 6/condition. Data are represented as mean ± SEM; two-tailed Student's t test, *$p < 0.05$ compared with Ctrl. n.s., not significant.

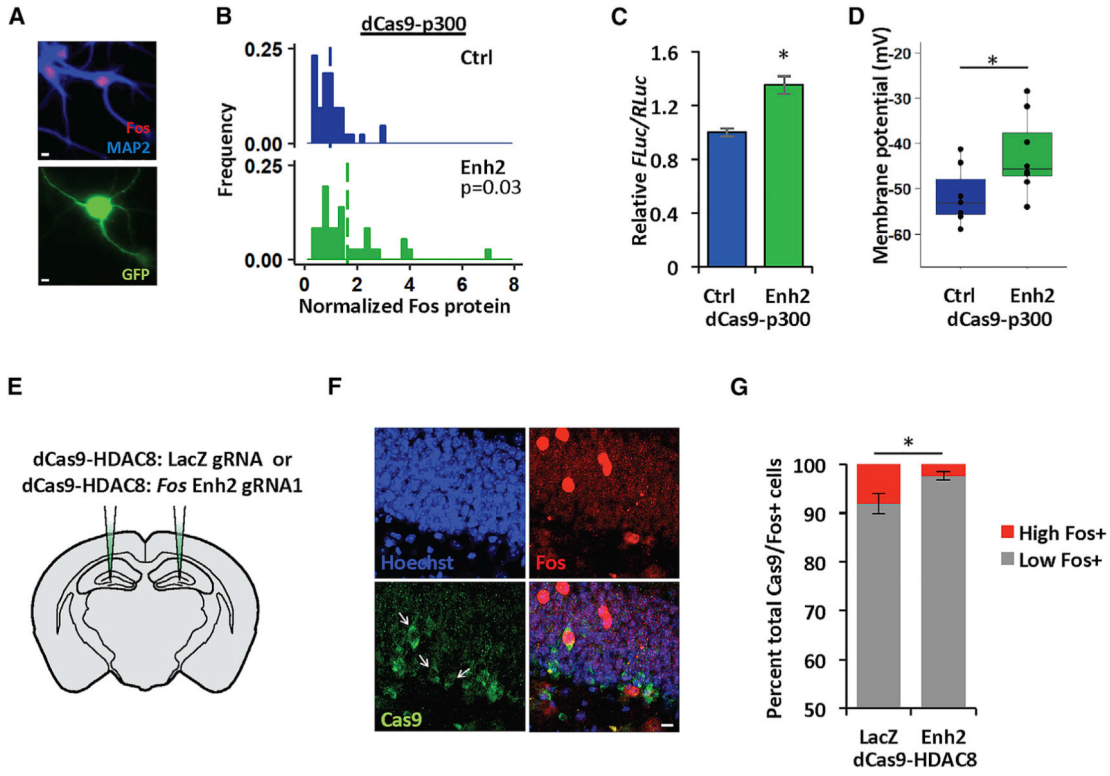

Figure 7. Local Regulation of *Fos* Enhancer Acetylation Tunes Fos Expression and Function in Cultured Neurons and *In Vivo*

(A) Representative immunohistochemistry (IHC) image of hippocampal neurons transfected with dCas-p300 and gRNAs.

(B) Observed distribution of Fos protein levels in cultured mouse neurons cotransfected with dCas-p300, along with either a Ctrl plasmid or a pool of gRNAs targeted to *Fos* Enh2. Data were analyzed by Kolmogorov-Smirnov test. p = 0.04. Ctrl, n = 43; Enh2, n = 36 neurons from 3 biological replicates. Dashed lines show average protein expression for each group. Scale bar, 5 μm.

(C) Firefly luciferase (*FLuc*) mRNA to Renilla luciferase (RLuc) mRNA levels in N2A cells cotransfected with 3xAP-1-FLuc, pTK-renilla luciferase, and dCas-p300, along with either a Ctrl gRNA plasmid or a pool of gRNAs targeted to *Fos* Enh2. The FLuc mRNA levels were normalized for each well to cotransfected RLuc mRNA levels. $p < 0.01$. n = 6/condition. Data are represented as mean ± SEM. *$p < 0.05$ compared with Ctrl.

(D) Box-and-whiskers plot of resting membrane potential (in millivolts) in mouse hippocampal neurons that were transfected with dCas-p300, along with either aCtrl plasmid or a pool of gRNAs targeted to *Fos* Enh2. Ctrl, n = 7; Enh2, n = 8 neurons from 2 biological replicates. Two-tailed Student's t test, p = 0.04. *$p < 0.05$ compared with Ctrl.

(E) Stereotaxic injection of dCas9-HDAC8 lentiviruses in the dorsal hippocampus of adult mice.

(F) Representative images of Fos (red) and Cas9 (green) immunostaining in virally infected regions of dentate gyrus.

(G) Percent distribution of high (red) and low (gray) Fos+ neurons among all dCas9-HDAC8+/Fos+ neurons from LacZ- or Enh2-targeted sides of the brain. Error bars show

SEM. n = 8 LacZ and 7 Enh2 hemispheres from 8 mice. Total Fos+/Cas9+ nuclei: LacZ, 325; Enh2, 276. *p < 0.05.

KEY RESOURCES TABLE

REAGENT or RESOURCE	SOURCE	IDENTIFIER
Antibodies		
Chicken anti-c-Fos	This paper	N/A
Chicken polyclonal anti-MAP2	EMD Millipore	Cat# AB5543; RRID:AB_571049
Goat polyclonal anti-Mouse IgG1	Biotium	Cat# 20253; RRID:AB_10852667
Mouse monoclonal anti-Actin	EMD Millipore	Cat# MAB1501; RRID:AB_2223041
Mouse monoclonal anti-c-FOS	EnCor	Cat# MCA-2H2; RRID:AB_2571561
Mouse monoclonal anti-FLAG (M2)	Sigma-Aldrich	Cat# F3165; RRID:AB_259529
Mouse monoclonal anti-POLR2A (8WG16)	Thermo Fisher Scientific	Cat# MA1-26249; RRID:AB_795353
Rabbit polyclonal anti-BRD4	Bethyl	Cat# A301-985A; RRID:AB_1576498
Rabbit polyclonal anti-GAD65	EMD Millipore	Cat#ABN101
Rabbit polyclonal anti-H3K27ac	Abcam	Cat# ab4729; RRID:AB_2118291
Rabbit polyclonal anti-RNA polymerase II CTD repeat YSPTSPS (phospho S2)	Abcam	Cat# ab5095; RRID:AB_304749
Rabbit polyclonal anti-Sp Cas9	EnCor	Cat# RPCA-C S9-Sp; RRID:AB_2744685
Bacterial and Virus Strains		
dCas9-HDAC8 *lacZ* gRNA Lentivirus	This paper	N/A
dCas9-HDAC8 *Fos* Enh2 gRNA1 Lentivirus	This paper	N/A
Chemicals, Peptides, and Recombinant Proteins		
(+)−JQ1	Sigma-Aldrich	Cat# SML1524
Forskolin	Sigma-Aldrich	Cat# F3917
Ribonucleoside Vanadyl Complex	NEB	Cat# S1402
Tetrodotoxin citrate	Tocris	Cat# 1069
Trichostatin A	Sigma-Aldrich	Cat# T8552
Critical Commercial Assays		
Absolutely RNA Miniprep Kit	Agilent	Cat#400800
EZ-ChIP	EMD Millipore	Cat#17–371
Lipofectamine 2000	Thermo Fisher Scientific	Cat# 11668019
Lipofectamine 3000	Thermo Fisher Scientific	Cat# L3000015
SuperScript™ II Reverse Transcriptase	Invitrogen	Cat# 18064
Deposited Data		
ChIP-seq H3K4me3 from e16.5 mouse forebrain	ENCODE Project Consortium	GEO: GSE82453
ChIP-seq H3K4me1 from e16.5 mouse forebrain	ENCODE Project Consortium	GEO: GSE82464
ChIP-seq H3K27ac from e16.5 mouse forebrain	ENCODE Project Consortium	GEO: GSE82690
Total RNA-seq from e16.5 mouse forebrain	ENCODE Project Consortium	GEO: GSE78323

REAGENT or RESOURCE	SOURCE	IDENTIFIER
Experimental Models: Cell Lines		
Neuro2a	ATCC	Cat# CCL-131
Experimental Models: Organisms/Strains		
CD-1 IGS mice	Charles River Laboratories	Strain code 022
C57BL/6J mice	The Jackson Laboratory	Stock #000664
Oligonucleotides		
Guide RNA sequences for CRISPR/Cas9, see Table S3.	This paper	N/A
Primers for qPCR, see Table S4.	This paper	N/A
Primers for ChIP-qPCR, see Table S5.	This paper	N/A
Recombinant DNA		
pcDNA-dCas9-p300 Core	Hilton et al., 2015	Addgene #61357
pcDNA-dCas9-p300 Core (D1399Y)	Hilton et al., 2015	Addgene #61358
Lentiviral-dCas9-HDAC8	This paper	N/A
Lentiviral gRNA vector	This paper	N/A
pRL-TK Renilla Luciferase Ctrl Reporter Vector	Promega	Cat# E223A
3xAP-1pGL3	Vasanwala et al., 2002	Addgene #40342
Software and Algorithms		
Stellaris RNA FISH Probe Designer	LGC Biosearch Technologies	https://www.biosearchtech.com/Account/Login?return=/stellaris-designer
MetaMorph	Molecular Devices	RRID:SCR_002368
FISH-Quant	Mueller et al., 2013	http://code.google.com/p/fish-quant/
BayFish	Gómez-Schiavon et al., 2017	https://github.com/mgschiavon/BayFish
Patchmaster	HEKA Elektronik	RRID:SCR_000034
Fiji	Schindelin et al., 2012	RRID:SCR_002285
Igor Pro	WaveMetrics	RRID:SCR_000325
MATLAB	MathWorks	RRID:SCR_001622
NIS-Elements	Nikon	RRID:SCR_014329